Experimental Evaluation of Hydrodynamic Characteristics of New Propulsion System Using Urethane Belt Drive

By

Md. Tariq Wazed Akash

ID: 1012008

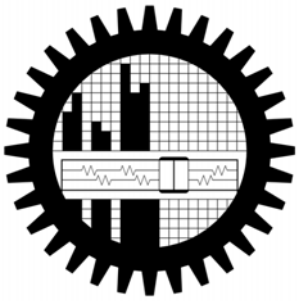

Department of Naval Architecture and Marine Engineering

Bangladesh University of Engineering and Technology

Dhaka-1000

February 2017

Experimental Evaluation of Hydrodynamic Characteristics of New Propulsion System Using Urethane Belt Drive

A thesis submitted by

Md. Tariq Wazed Akash

ID: 1012008

Thesis Supervisor

Professor Dr. Md. Mashud Karim

This thesis submitted in a partial fulfillment of the requirements for the degree of

BACHELOR OF SCIENCE IN
NAVAL ARCHITECTURE AND MARINE ENGINEERING

at the

Bangladesh University of Engineering and Technology
Dhaka-1000, Bangladesh
February 2017

Experimental Evaluation of Hydrodynamic Characteristics of New Propulsion System Using Urethane Belt Drive

DECLARATION

This is to certify that the thesis is done by me and has not been submitted anywhere else for the award of any degree or diploma.

_____

Signature of the Student

Md. Tariq Wazed Akash
(ID: 1012008)

ACKNOWLEDGMENT

This thesis is the prime result of my bachelor studies which is undertaken since November 2016 to February 2017 at the Bangladesh University of Engineering and Technology (BUET). My funding has been solely provided by the Department of Naval Architecture & Marine Engineering under the wise and helpful supervision of Professor Dr. Mashud Karim.

Above all the circumstances considering aside, I would like to thank my supervisor Professor Dr. Mashud Karim for not only giving me the necessary guidelines regarding to the thesis but also for helping me in the thesis project as a mentor and as a skillful teammate. I would not have completed the thesis in due time with anticipated results if it was not for him, precisely. Through his cooperation, suggestions as well as righteous encouragement, I have set my mark on the main goal of this thesis project.

Furthermore, I would like to give thanks to our honorable head of the department, Professor Dr. Goutam Kumar Saha and other respected faculties of the Department of Naval Architecture and Marine Engineering, BUET for their kind support.

Finally, I would like to express my gratitude to all my family and friends for their support and patience and especially to my parents for their continued backing up in all my choices. All the work put into this thesis would not have been possible without a brother as well as a friend that shares the shoulders. Thank you Siam, for your creativity, support and for being right beside.

Dhaka, February 28th , 2017 **Md. Tariq Wazed Akash**

ABSTRACT

Hydrodynamic characteristics of new propulsion system using urethane belt drive have been evaluated experimentally in this thesis. A small scale model has been developed and a BLDC motor has been used to rotate the urethane belt. In order to measure hydrodynamic forces, a load cell was used. The calibration of the load cell was done with known loads. All these processes have been controlled over by written codes at Arduino. This model was tested in an enclosed boundary (water trough) and the density of water was taken as similar as fresh water. The input power has been expressed as ampere and output thrust as newton by the Arduino module. Iterative average theory is applied here, in order to mining all the gathered data and to finding out the most approximated values at different stages of the calculations. After analyzing the experimental data, the efficiency of the model has slightly been increased up to 11.07% approximately. This increment of efficiency has been analyzed for single screw-propulsion and coupled-screw propulsion and therefore plotted as the efficiency curve. The experimental results are compared with theoretical results and found satisfactory.

NOMENCLATURES

Symbol	*Definition with S.I. Units*
dx, dy, dz	*Control volume dimensions (m)*
ρ	*Density of fluid (kgm^{-3})*
Θ	*Propeller pitch angle (radian)*
b	*Propeller chord length (m)*
V_P	*Propeller's rotational speed (r.p.m.)*
V_1, V_2, V_3	*Axial velocity of water (ms^{-1})*
V_A, V_B, V_C	*Axial velocity of fluid at A,B & C points (ms^{-1})*
V_R	*Resultant velocity of control volume (ms^{-1})*
h, z	*Axial projected lengths of blade (m)*
T	*Thrust of propeller (N)*
A	*Total Area of propulsion (m^2)*
R	*Propeller radius from hub (m)*
r	*Radius of the hub (m)*
L	*Length of coupling chain (m)*
d	*Distance between blades attachment (m)*
D	*Propeller diameter (m)*
n	*Propeller speed (rev/s)*
Nm	*Torque (Q)*
μ	*Fluid viscosity (m^2/s)*
K	*Fluid bulk elasticity modulus (N/m^2)*
P	*Pressure (Nm^{-2})*
C_T	*Thrust Coefficient*
C_P	*Pressure Coefficient*
C_L	*Lift Coefficient*
η_0	*Efficiency of Propeller*
α	*Angle of attack*
β	*Hydrodynamic pitch angle*
Γ	*Vortex Strength Function*
A_R	*Aspect Ratio*
C_F	*Coefficient of Friction*
K_T	*Thrust Coefficient in Non-dimensional Form*
K_Q	*Torque Coefficient*
J	*Advance Coefficient*

LIST OF FIGURES

1.	Patent of Chain Propeller by G. Hart…….	14
2.	Patent of Chain Propeller by N.W. French……	15
3.	Patent of Chain Propeller by E.N. Kerr…….	16
4.	Archimedean Screw……...	18
5.	Voith-Schneider Propeller Motion……	23
6.	Actuator Disc Geometry……	24
7.	Blade Elemental Geometry……	26
8.	Pressure Differentials on A Blade…….	27
9.	Lift vs. Angle of Attack Curve……...	28
10.	Circulation of Fluids Around Blade Element……	30
11.	Vortex Distribution Around Blade Element……..	31
12.	Fluid Particle (control volume) Flows Over A Blade Section……...	35
13.	Electronic Modules For Experimental Setup…….	40
14.	BLDC Motor……..	41
15.	ESC (Electronic Speed Control)……	42
16.	Arduino Chipset Schematics (Labeled)…….	43
17.	Interface of the Arduino programming editor (IDE)…….	45
18.	Load Cell……...	47
19.	Lithium Polymer Battery……..……..	48
20.	HX711 Module……..	50
21.	Pin Descriptions of HX711 Module……..	50

22. Connectivity Diagram of Different Modules……. 51

23. 3D Output of Coupled Propeller (Perspective)…….. 52

24. 3D Output of Coupled Propeller (Top)…….. 53

25. 3D Output of Coupled Propeller (Front)……... 53

26. 3D Output of Coupled Propeller (Right)……... 54

27. 3D Output of Elemental Propeller Blade (Perspective)……. 54

28. 3D Output of Elemental Propeller Blade (Right)…….. 55

29. 3D Output of Elemental Propeller Blade (Top)……. 55

30. 3D Output of Elemental Propeller Blade (Front)…….. 56

31. 3-D Printed Propeller Blades…… 56

32. Polyurethane Belts (Ring Type)…… 58

33. Modules Assembly……..……... 59

34. Propellers Underwater (Tank Test)……... 60

35. Source Code for ESC Calibration……..……... 61

36. Source Code for HX711 Calibration : Page-1……... 62

37. Source Code for HX711 Calibration : Page-2……... 63

38. Source Code for HX711 Calibration : Page-3……... 64

39. Source Code for HX711 Calibration : Page-4……... 65

40. Source Code for HX711 Calibration : Page-5……... 66

41. Source Code for HX711 Calibration : Page-6……... 67

42. Source Code for BLDC Motor Calibration : Page-1……...…….. 68

43. Source Code for BLDC Motor Calibration : Page-2……...…….. 69

44. Source Code for BLDC Motor Calibration : Page-3……...…….. 70

45. Source Code for BLDC Motor Calibration : Page-4……...…….. 71

46. Source Code for BLDC Motor Calibration : Page-5……. 72

47. Source Code for BLDC Motor Calibration : Page-6……..…… 73

48. Source Code for BLDC Motor Calibration : Page-7…….. 74

49. Source Code for BLDC Motor Calibration : Page-8…….. 75

50. Measurement Of Consumed Power & Given Thrust by Multimeter & Load cell..... 77

51. Thrust (N) Vs. Speed (rpm%) Curve for Single Screw…….…… 85

52. Thrust (N) Vs. Speed (rpm%) Curve for Coupled Screw…….…… 90

53. Propeller Efficiency Curve for Single Screw……...……..… 93

54. Propeller Efficiency Curve for Coupled Screw……...……..… 94

LIST OF TABLES

1.	Technical Specification of BLDC Motor……	41
2.	Technical Specification of Arduino Chipset……...	44
3.	Technical Specification of Load cell……	47
4.	Technical Specification of Urethane Belts……..	58
5.	Calibration of Load cell Reading (0 g)…….	79
6.	Calibration of Loadcell Reading (244 g)…….	80
7.	Interpolation for $X_{L.C.}$ Value……	82
8.	Thrust reading for Single Screw……..	82
9.	Thrust vs. Speed% Table for Single Screw…….	84
10.	Performance Table for Single Screw……...	87
11.	Thrust reading for Coupled Screw……...	88
12.	Thrust vs. Speed% Table for Coupled Screw……..	90
13.	Performance Table for Coupled Screw…….....	92

TABLE OF CONTENTS

ACKNOWLEDGMENT 4
ABSTRACT 5
NOMENCLATURES 6
LIST OF FIGURES 7
LIST OF TABLES 10

Chapter : 01 || INTRODUCTION 14

Chapter : 02 || BACKGROUND 18
2.1 Prehistory 18
2.2 Archimedean Screw 18
2.3 Early Inventions 19
2.4 Screw propellers 19
2.5 Propulsion System 21
2.5.1 Fixed Pitch Propellers 21
2.5.2 Ducted Propellers 21
2.5.3 Skewed Propellers 21
2.5.4 Podded & Azimuth Propulsors 21
2.5.5 Contra-Rotating Propellers 22
2.5.6 Controllable pitch propellers 22
2.5.7 Water-Jet Propulsion 23
2.5.8 Voith–Schneider Propeller : Vertical Axis Cyclorotor 23

Chapter : 03 || CONVENTIONAL PROPELLER THEORIES 24
3.1 Momentum Theory 24
3.2 Blade Element Theory 26
3.3 Profile Characteristics 27
3.4 Lifting Line Theory 30
3.4.1 Special case of elliptical loading: 33

Chapter : 04 || MATHEMATICAL ANALYSIS 34
4.1 Assumptions 34
4.2 Derivation of the Equation for Thrust 35
4.3 Validation by Dimensional Analyses 38

Chapter : 05 || EXPERIMENTAL SETUP 40
5.1 Electronic Modules 40
5.1.1 BLDC (Brushless Direct Current) Motor 41
5.1.2 ESC (Electronic Speed Control) Circuit 42
5.1.3 Arduino (Uno) 433
5.1.4 Load Cell (5 Kg) 466
a) Single-Point Load Cell 477
5.1.5 Li-Po (Lithium-Polymer) Battery 488
5.1.6 HX711 Module (The Amplifier) 49
5.2 Connectivity Arrangements 51
5.3 Propeller Blades 522
5.3.1 Conceptual Output 522
5.3.2 Object File (Printable Output) 544
5.3.3 Printed Blades (Elemental Unit of Propeller) 566
5.4 Urethane Belt Drive 588
5.5 Assembled Modules in a Glimpse 59
5.6 The “Sketch” for Thrust Estimation 60
5.6.1 ESC Calibration Codes 611
5.6.2 HX711 Module Calibration Code 622
5.6.3 BLDC Motor Calibration Codes 688

Chapter : 06 || RESULTS AND DISCUSSION 766
6.1 Data and Results validation 766
6.2 Data Obtaining Methodology 766
6.3 Iterative Average Theory 777
6.4 Calibration of Load Cell 788

6.5 Performance Investigation of Single Screw 822
6.5.1 Data Mining & Curve Generation 822
6.5.2 Performance Calculation 855
6.6 Performance Investigation of Coupled Screw 888
6.6.1 Data Mining & Curve Generation 888
6.6.2 Performance Calculation 911
6.7 Comparative Performance Analyses 933

Chapter : 07 || CONCLUSION AND RECOMMENDATION 955
7.1 Conclusion 955
7.2 Recommendation 955

REFERENCES 977

Chapter : 01
INTRODUCTION

Marine vessels are fitted with many devices to help itself in case of maneuver, motion and control and berthing. Whereas, propulsive device is the main key to all of these activities, this device can be of various types and purposes, such as; single screw, twin screw, ducted propeller, bow-thruster, rexpeller, air-jet, etc. This thesis is all about the investigation for performance of a comparatively unconventional propulsion device which is made of two shafts with a number of blades and this is more than the sum of the blades that twin-screw propeller can have in a combination instead. An idea very similar to this research was first brought to light by G. Hart (1884) [1]. But this was a patent and neither any experimental works had been initialized back then nor near past to measure the authenticity of the device. That patent was followed with or without modifications by other technical persons afterwards. Some of these patents are given below chronologically to build up the clear idea of what it is being discussed throughout the thesis.

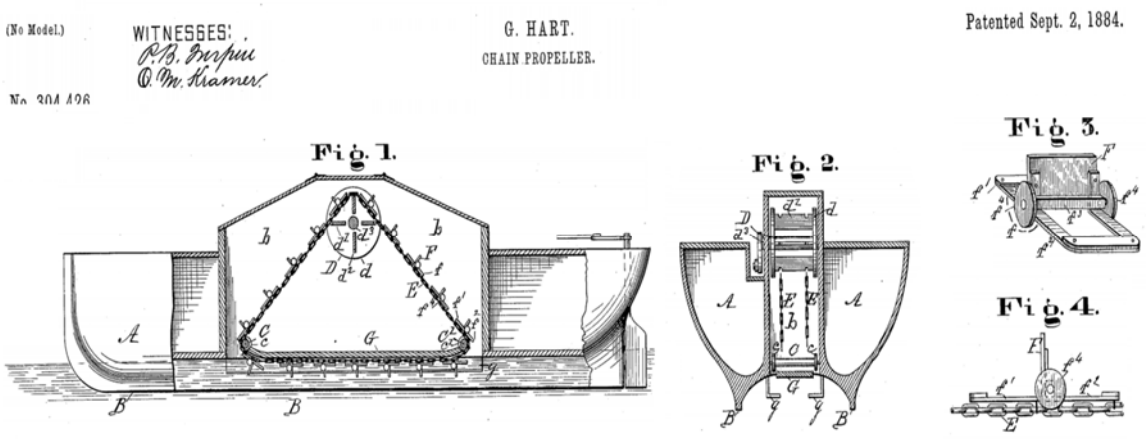

Figure 1: Patent of Chain Propeller by G. Hart.

Above patent was the work of G. Hart which was first copyrighted on September 2, 1884. Five years later, another modification was patented by N.W. French [2]:

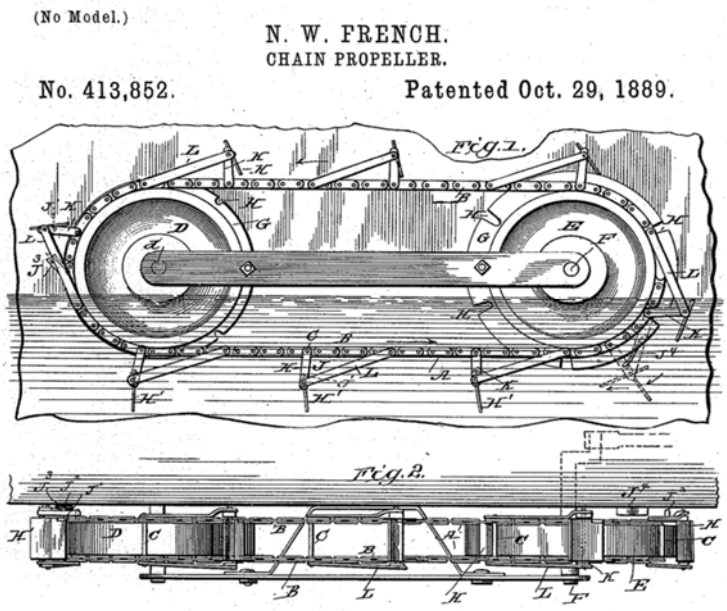
(No Model.)

N. W. FRENCH.

CHAIN PROPELLER.

No. 413,852. Patented Oct. 29, 1889.

Fig. 1.

Fig. 2.

Figures 2: patent of Chain Propeller by N.W. French.

This was much more visually similar to this thesis's model. After that more than twenty individual patents had been copyrighted. But those patents did not have any sort of proper experimental proofs to be stated as legit in the sense of engineering science.

If it is to understand the inner mechanism of these devices entirely, then this is to watch through from the perspective of a technical viewpoint. Basically, the two shafts being like holding still at a certain distance from each other whereas the distance between these, is proportional to the radius of the propeller hub, radius of the blade and the breadth of the ship. An important point to be noted that, only one of the shaft will get to attach through the engine's gear box and it will rotate as the engine starts when the other shaft will only follow the first shaft in case of rotation. The fundamental meaning of the system is that, two screws can be used from the consumed power which is only intended for one screw [3]. So, when the rotation of shafts begins, the wrapped-over belt around the propeller hubs will also start to move along. Adjoining blades on the belt also make revolution from one shaft to other and again the process happens from the start. In other words, it is usually a **"Cam-Follower"** system from mechanics of machines. So the propulsion mechanism goes on by the linking motion of these two separate propeller shafts which work as one system [4].

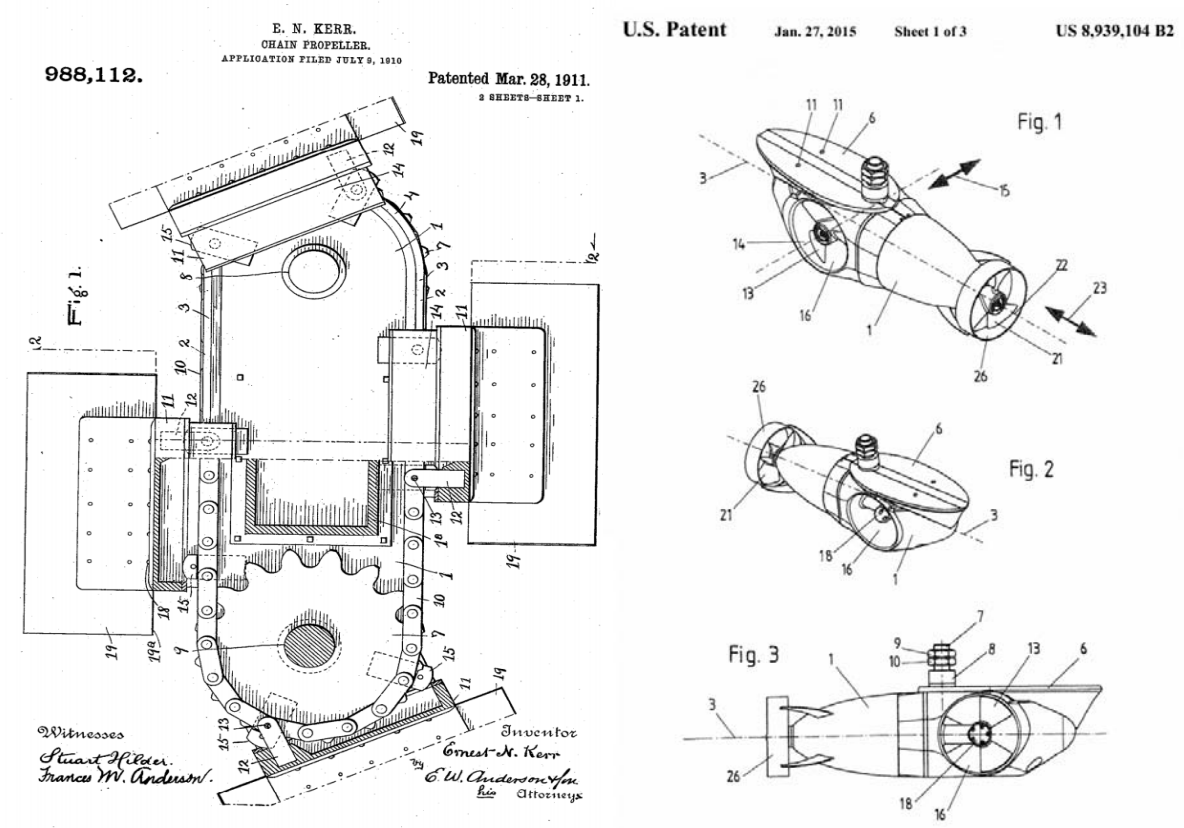

Figure 3: Patent of Chain Propeller by E.N. Kerr.

The efficiency of the device depends not only on the input of mechanical power varieties but also depends on some cases like; water characteristics, weather condition, forward or afterward motion, deadweight of the vessel, turning radius, maneuvering torque of rudder, rolling-pitching-heaving motion, etc [5]. But, in case of a model, the efficiency more likely to depend on the ratio of the mechanical power (given) and the thrust (delivered) [6]. So, for research and analytical purpose, a model had been built and the efficiency parameters will be measured from this model. Primarily, it is to measure the current consumption of the device while rotating and then the input power to be calculated by sorting out how much voltage of battery has been used for the device; this will give the denominator of the efficiency ratio. On the other hand, the numerator will be force or thrust delivered by the propellers, which to be measured by using load-cell readings with the help of ***Arduino*** based console. Finding the ratio of efficiency is the main objective of the ongoing research project with some subordinate objectives.

The research topic along with the following areas will be highlighted for the new experimental device:

a) Estimation of thrust (T) after coupling with the belt drive,
b) Estimation of torque (Q) and generating comparative tables,
c) Comparison of rpm, thrust, torque between single-screw and twin-screw,
d) Developing the efficiency curves (Thrust vs. Percentage of velocity).

According to the operational philosophy of propulsion system will affect three important aspects of the operation of a marine vessel and these are: safety, economy, and performance. If any system can maximize performance and safety, minimizing economic expenses at the same time, then the system is to be said operationally feasible. In other sense, if performance reaches up having no extra economic expenses and safety stays in stable position, then it is also likely to be said another feasible operational system.

Chapter : 02
BACKGROUND

2.1 Prehistory

The main theory that is employed in using a screw propeller is used in sculling. It is part of the skill of propelling a Venetian gondola but was used in a less refined way in other parts of Europe and probably elsewhere. For example, propelling a canoe with a single paddle using a "pitch stroke" or side slipping a canoe with a ***"scull"*** involves a similar technique. In China, sculling, called ***"lu"***, was also used by the 3rd century AD. In ***"sculling"*** [7], a single blade is moved through an arc, from side to side taking care to keep presenting the blade to the water at the effective angle. The innovation introduced with the screw propeller was the extension of that arc through more than 360° by attaching the blade to a rotating shaft. Propellers can have a single blade, but in practice there is nearly always more than one so as to balance the forces involved.

Figure 4: Archimedean screw.

2.2 Archimedean Screw

The origin of the screw propeller starts with Archimedes, who used a screw to lift water for irrigation and bailing boats, so famously that it became known as Archimedes' screw. "Archimedes Screw" is a machine that can move water masses with much less effort than lifting it up. It was invented by the Greek scientist Archimedes, between 287 B.C. and 212 B.C. The Archimedes screw is an ancient invention that continues to be important in the

modern world. Leonardo da Vinci adopted the principle to drive his theoretical helicopter, sketches of which involved a large canvas screw overhead.

2.3 Early Inventions

In 1784, Paucton [8] proposed a gyrocopter-like aircraft using similar screws for both lift and propulsion. At about the same time, James Watt proposed using screws to propel boats, although he did not use them for his steam engines. This was not his own invention, too good and Hays had patented it a century earlier, and it had become a common use as a means of propelling boats since that time.

By 1827, Czech-Austrian inventor Josef Ressel had invented a screw propeller which had multiple blades fastened around a conical base. He had tested his propeller in February 1826 on a small ship that was manually driven. He was successful in using his bronze screw propeller on an adapted steamboat (1829). His ship *"Civetta"* with 48 gross registers tons, reached a speed of about six knots (11 km/h). This was the first ship successfully driven by an Archimedes screw-type propeller. After a new steam engine had an accident (cracked pipe weld) his experiments were banned by the Austro-Hungarian police as dangerous. Josef Ressel was at the time a forestry inspector for the Austrian Empire. But before this he received an Austro-Hungarian patent (license) for his propeller (1827). He died in 1857. This new method of propulsion was an improvement over the paddlewheel as it was not so affected by either ship motions or changes in draft as the vessel burned coal [9].

John Patch, a mariner in Yarmouth, Nova Scotia developed a two-bladed, fan-shaped propeller in 1832 and publicly demonstrated it in 1833, propelling a row boat across Yarmouth Harbor and a small coastal schooner at Saint John, New Brunswick, but his patent application in the United States was rejected until 1849 because he was not an American citizen. His efficient design drew praise in American scientific circles, but by this time there were multiple competing versions of the marine propeller.

2.4 Screw propellers

Although there was much experimentation with screw propulsion until the 1830s, few of these inventions were pursued to the testing stage, and those that were, proved unsatisfactory for one reason or another. Smith's original 1836 patent for a screw propeller of two full turns.

Therefore, he would later revise the patent, reducing the length to one turn. In 1835, two inventors in Britain, John Ericsson and Francis Pettit Smith, began working separately on the problem. Smith was first to take out a screw propeller patent on 31 May, while Ericsson, a gifted Swedish engineer then working in Britain, filed his patent six weeks later. Smith quickly built a small model boat to test his invention, which was demonstrated first on a pond at his Hendon farm, and later at the Royal Adelaide Gallery of Practical Science in London, where it was seen by the Secretary of the Navy, Sir William Barrow. Having secured the patronage of a London banker named Wright, Smith then built a 30-foot, 6-horsepower canal boat of six tons burthen called the Francis Smith, which was fitted with a wooden propeller of his own design and demonstrated on the Paddington Canal from November 1836 to September 1837. By a fortuitous accident, the wooden propeller of two turns was damaged during a voyage in February 1837, and to Smith's surprise the broken propeller, which now consisted of only a single turn, doubled the boat's previous speed, from about four miles an hour to eight. Smith would subsequently file a revised patent in keeping with this accidental discovery. In the meantime, Ericsson built a 45-foot screw propelled steamboat, Francis B. Ogden in 1837, and demonstrated his boat on the River Thames to senior members of the British Admiralty, including Surveyor of the Navy Sir William Symonds. In spite of the boat achieving a speed of 10 miles an hour, comparable with that of existing paddle steamers, Symonds and his entourage were unimpressed. The Admiralty maintained the view that screw propulsion would be ineffective in oceangoing service; while Symonds himself believed that screw propelled ships could not be steered efficiently. Following this rejection, Ericsson built a second, larger screw-propelled boat, the Robert F. Stockton, and had she sailed in 1839 to the United States, where he was soon to gain fame as the designer of the U.S. Navy's first screw-propelled warship, USS Princeton. Apparently aware of the Navy's view that screw propellers would prove unsuitable for seagoing service, Smith determined to prove this assumption wrong. In September 1837, he took his small vessel (now fitted with an iron propeller of a single turn) to sea, steaming from Blackwall, London to Hythe, Kent, with stops at Ramsgate, Dover and Folkestone. On the way back to London on the 25th, Smith's craft was observed making headway in stormy seas by officers of the Royal Navy. The Admiralty's interest in the technology was revived, and Smith Wen courage to build a full size ship to more conclusively demonstrated the technology's effectiveness.

2.5 Propulsion System

There have been developed so many different types of propellers [10] around the globe. Among these propulsion devices, only few important types are discussed in the following articles.

2.5.1 Fixed Pitch Propellers

This type of propeller is developed at the early stage of the screw propulsion era. At this propeller, the blade cannot be pitched in variance with the change of the rotational torque. The blades are welded or riveted at the root of the hub.

2.5.2 Ducted Propellers

A circular duct is covered around the propeller of which diameter is slightly greater than the propeller diameter. That is why the propeller can revolute along with the time without the external force acting on it. Besides, the circulation of the blades cannot affect the propeller inside the ducts.

2.5.3 Skewed Propellers

There are practically two types of skew: Balanced and unbalanced. The balanced type is skew within lesser limits; where the generator line intersects the datum line at least two points. These types of ship propellers are known as 'moderately skewed' [11]. On the other hand, unbalanced skew is a higher degree of deviation where the generator line intersects the reference line at not more than one point (considerably higher range of skew). They are said to be 'heavily skewed'.

2.5.4 Podded and Azimuth Propulsions

Azimuth thrusters have been in common use for many years and can have either non-ducted or ducted propeller arrangements. The essential difference between the azimuth and podded

propellers lies in where the engine or motor driving the propeller is sited. If the motor is sited in the ship's hull then the system would be termed azimuth propulsion and most commonly the mechanical drive would be of a Z or L type to the propeller shaft. Frequently, the drive between the vertical and horizontal shafts is via spiral bevel gears.

2.5.5 Contra-Rotating Propellers

The contra-rotating propeller principle, comprising two coaxial propellers sited one behind the other and rotating in opposite directions, has traditionally been associated with the propulsion of aircraft though it is now often used for marine propulsion. Contra-rotating propulsion systems have the hydrodynamic advantage of recovering part of the slipstream rotational energy which would otherwise be lost to a conventional single screw system [12]. Furthermore, because of the two propeller configuration, contra-rotating propellers possess a capability for balancing the torque reaction from the propulsor which is an important matter for torpedo and other similar propulsion problems. In marine applications of contra-rotating propulsion it is normal for the aftermost propeller to have a smaller diameter than the forward propeller and, in this way, accommodate the slipstream contraction effects. Similarly, the blade numbers of the forward and aft propellers are usually different; typically, four and five for the forward and aft propellers, respectively.

2.5.6 Controllable Pitch Propellers

Unlike fixed pitch propellers whose only operational variable is rotational speed, the controllable pitch propeller provides an extra degree of freedom in its ability to change blade pitch. However, for some propulsion applications, particularly those involving shaft-driven generators, the shaft speed is held constant, thus reducing the number of operating variables again to one. While this latter arrangement is very convenient for electrical power generation it can cause difficulties in terms of the cavitation characteristics of the propeller by inducing back and face cavitation at different propulsion conditions.

2.5.7 Water-Jet Propulsion

The origin of the water-jet principle can be traced back to 1661, when Toogood and Hayes produced a description of a ship having a central water channel in which either a plunger or centrifugal pump was installed to provide the motive power [8]. In more recent times water-jet propulsion has found considerable application on a wide range of small high-speed craft while its application to larger craft is growing with tunnel diameters of upwards of 2 m being considered. The principle of operation of the present-day water-jet is that in which water is drawn through a ducting system by an internal pump which adds energy after which the water is expelled aft at high velocity. The unit's thrust is primarily generated as a result of the momentum increase imparted to the water.

2.5.8 Voith–Schneider Propeller : Vertical Axis Cyclorotor

Voith–Schneider propeller (Cycloidal) propeller development started in the 1920s, initially with the Kirsten–Boeing and subsequently the Voith–Schneider designs. It is interesting to note that the Kirsten–Boeing design was very similar in its hydrodynamic action to the horizontal waterwheel developed by Robert Hooke some two and half centuries earlier in 1681.

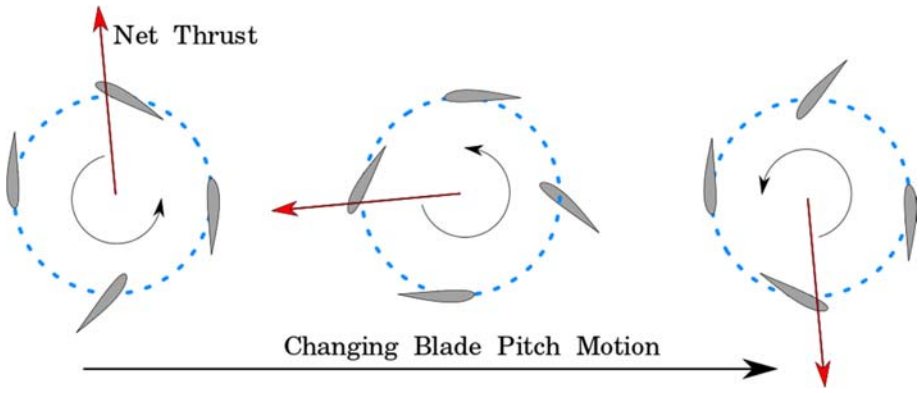

Figure 5: Voith-Schneider Propeller

The cycloidal or vertical axis propellers basically comprise a set of vertically mounted vanes, six or eight in number, which rotate on a disc mounted in a horizontal or near horizontal plane. The vanes are constrained to move about their spindle axis relative to the rotating disc in a predetermined way by a governing mechanical linkage.

Chapter : 03
CONVENTIONAL PROPELLER THEORIES

This section has been combined with previous propeller theories on which the successive evolution of propellers had been happened. The ongoing experiment is closely dependent on these theories and with the help of some mathematical concepts; the model has been being upgraded day by day so far.

3.1 Momentum Theory

It was originally intended to provide an analytical means for evaluating ship propellers (Rankine 1865 & Froude 1885) [5]. Momentum Theory is also well known as ***Disk Actuator Theory***. Momentum Theory assumes that,

- The flow is inviscid and steady (ideal flow), therefore the propeller does not experience energy losses due to frictional drag,
- Also the rotor is thought of as an actuator disk with an infinite number of blades, each with an infinite aspect ratio,
- The propeller can produce thrust without causing rotation in the slipstream.

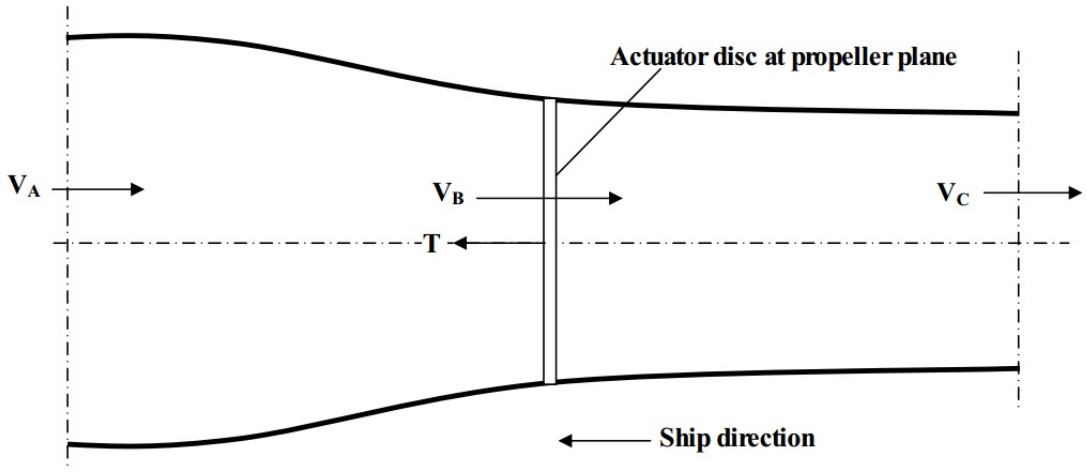

Figure 6: Actuator Disc geometry

From the basic thrust equation, it has been proved that half of the acceleration takes place before the propeller disc and the remaining half after the propeller disc. In other words the axial induced velocity at the propeller (u_a) is the half the axial induced velocity at the C. The propeller thrust is made non-dimensional with the propeller area and hence the inflow velocity V_A:

$$C_T = \frac{T}{\frac{\pi}{4}D^2 \frac{1}{2}\rho V_A^2} \tag{15}$$

Where, C_T is a thrust coefficient indicating the propeller loading.

The induced velocity in the slipstream represents energy supplied to the flow behind the propeller. This is due to the fact that the fluid gives way when a thrust is exerted to it. The loss of the energy is reflected in an efficiency which is lower than 1. To formulate the efficiency the propeller disk moves with a velocity V_A and exerts a force T. The power is TV_A. In the slipstream a velocity $2u_a$ is present. The efficiency of the propeller can be written as:

$$\eta_0 = \frac{1}{1+\frac{u_a}{V_A}}$$

$$or \tag{19}$$

$$\eta_0 = \eta_i = \frac{2}{1+\sqrt{1+C_T}}$$

This represents the maximum efficiency which is theoretically possible in an inviscid flow with a propeller not introducing any rotation in the slipstream. It is therefore called the ideal efficiency.

3.2 Blade Element Theory

The primary limitation of the ***momentum theory*** [6] is that it provides no information as to how the rotor blades should be designed so as to produce a given thrust. Also, profile drag losses are ignored. The blade-element theory is based on the assumption that each element of a propeller or rotor can be considered as an airfoil segment. Lift and drag are then calculated from the resultant velocity acting on the airfoil, each element considered independent of the adjoining elements. The thrust and torque of the rotor are obtained by integrating the individual contribution of each element along the radius.

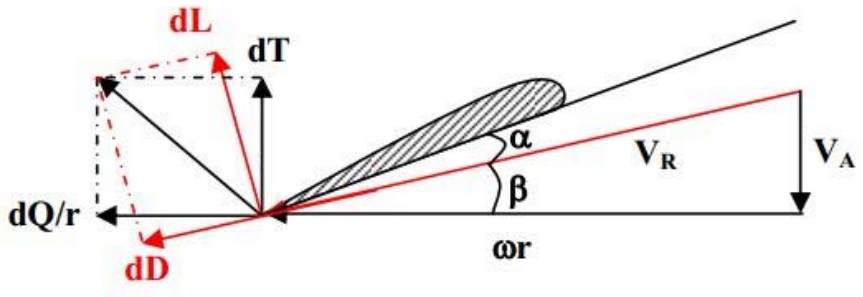

Figure 7: Blade Elemental Geometry

The thrust force of a blade can be obtained by integrating the **dT** over the radius **R** and the total thrust force is found by the multiplication of number of blades by the blade thrust force.

Similarly total torque can be obtained as:

$$T = Z\int_{r_h}^{R} dT dr = Z\int_{r_h}^{R} (dL\cos\beta - dD\sin\beta)dr \tag{20}$$

$$Q = Z\int_{r_h}^{R} dQ dr = Z\int_{r_h}^{R} dF r dr = Z\int_{r_h}^{R} (dL\sin\beta + dD\cos\beta) r dr \tag{21}$$

The propeller efficiency:

$$\eta = \frac{TV_A}{Q\omega} \tag{22}$$

3.3 Hydrodynamic Characteristics

A characteristic feature of a profile is to generate lift (L). This profile (lifting surface) in a flow also generates drag (D) and pitching moment (M). The lift is caused by the fact that the flow is forced to leave the profile smoothly at the tail. This is in turn an effect of viscosity which prevents the velocities from becoming extremely large at the tail. This condition is called Kutta condition. Basically it is a tangential flow at the tail, or equal pressure at both sides of the tail.

Let us consider a profile moving at a certain angle of attack through the fluid as in the figure below:

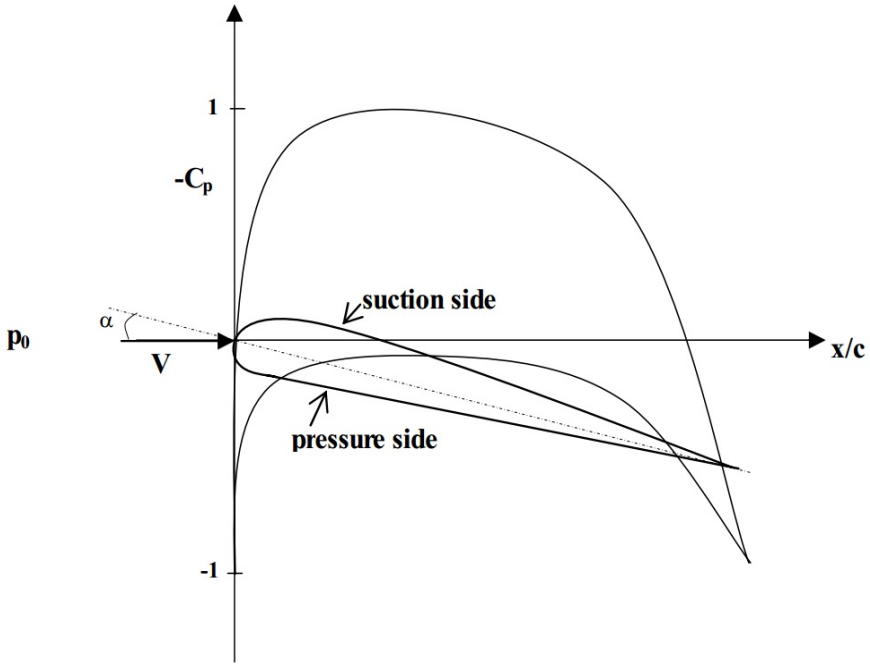

Figure 8: Pressure Distribution on a Propeller Blade

There is an inflow velocity at the angle of attack α . As a result of the inflow there is a certain pressure distribution over the surface of the profile [13]. When the pressure P_0 in the undistributed flow is changed, the pressure over the surface of the profile will also change with the same amount. The effect of the immersion h is neglected, because the profile is assumed to be nearly horizontal and a small angle of attack. The above theory shows that two stagnation points exist where the local velocity is zero. These stagnation points are called

forward and rear stagnation points. Typical pressure distribution on a profile is shown in the above figure. The pressure difference between suction side and pressure side is the loading of the profile. The integral of this loading distribution over the chord gives the lift force L on the profile. The lift coefficient can be given as:

$$C_L = \frac{L}{\frac{1}{2}\rho S V^2} \tag{26}$$

Where, *S* is an area (span times chord length). For a profile the lift coefficient per unit span is also used where S is replaced by the chord length c . A typical angle of attack versus C_L is shown in the figure below:

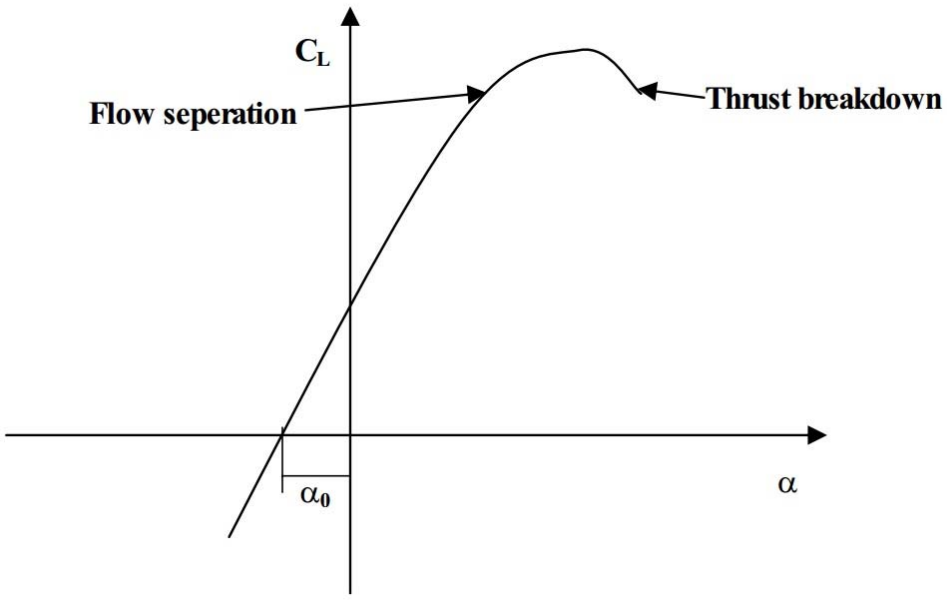

Figure 9: Left vs. Angle of Attack Curve

As can be seen in the above figure the lift coefficient C_L crosses the x-axis at the zero lift angle (α_0) where the profile generates no lift. This angle is determined by the camber of the profile and calculated as $\boldsymbol{\alpha_0} = \frac{2f_{\max}}{c}$. The slope of the lift curve ($\frac{\partial C_L}{\partial \alpha}$) is 2π for thin profiles.

At higher angles of attack the lift curve deviates from the linear theory and flow separation and thrust breakdown occur.

The term ideal angle of attack, α_i , is the angle of attack at which pressure around the leading edge is symmetrical In this case the flow direction at the leading edge is exactly in the direction of camber line. It is very important because at this angle the pressure close to the leading edge is maximum. Propeller blade sections are generally designed to operate at the ideal angle of attack.

The drag force is caused by the friction along the surface of the profile and is expressed in non-dimensional terms as:

$$C_D = \frac{D}{\frac{1}{2}\rho S V^2} \tag{28}$$

3.4 Lifting Line Theory

A simple solution for no-swept three-dimensional wings can be obtained by using Prandtl's lifting line model. For incompressible, inviscid flow, the wing is symbolized as a single bound vortex line located at the 1/4 chord position and an associated shed vortex sheet.

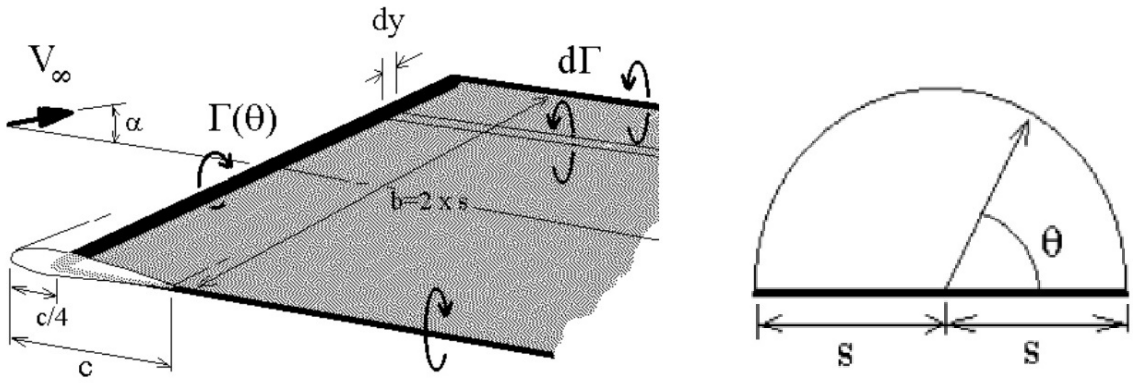

Figure 10: Circulation of Fluids Around Blade Element

The span-wise lift distribution is assumed to be elliptical with a small modification due to wing plan-form geometry. The assumed vortex line strength is thus a Fourier series approximation. The required strength of the distribution coefficients (A_n) for a given geometry and set of free-stream conditions can be calculated by applying a surface flow boundary condition. The equation used is based on the usual condition of zero flow normal to the surface. For 3D wings the condition is applied at several span-wise sections by matching flow and surface angles. The local flow angle of incidence for a 2-D section of the wing must be equal to the sum of the wing's angle of attack, the section twist and the down-wash induced flow angle. This down-wash component is caused by the induced flow from the trailing vortex [14] sheet.

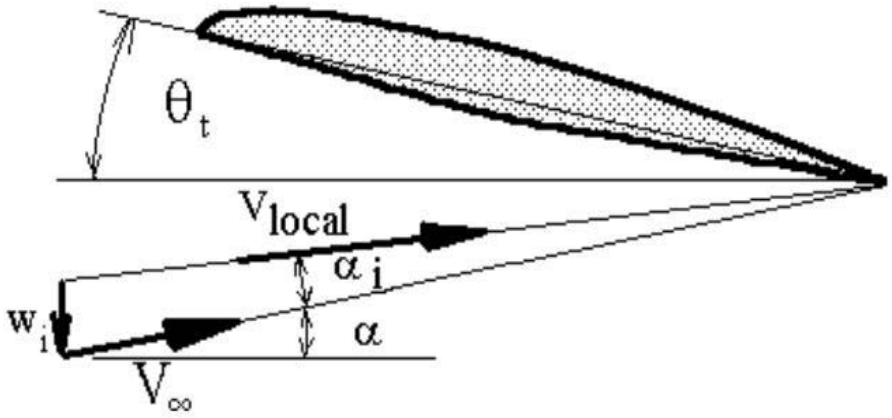

$$\alpha_{2\text{-}D} = \alpha - \alpha_i + \theta_t$$

$$\alpha_i = w_i / V_\infty$$

Figure 11: Vertex Distribution Around Blade Element

Where, α is the 3-D wing angle of attack, θ_t is the wing twist angle and w_i is the velocity induced by trailing vortex sheet. The vortex strength distribution in the trailing sheet will be a function of the changes in vortex strength along the wing span. The mathematical function describing the vortex sheet strength is thus obtained by differentiating the bound vortex distribution.

A solution for the magnitude of the Fourier coefficients A_1, A_2, A_3... is obtained by firstly predicting the down-wash velocity induced on the wing by the trailing sheet.

$$d\Gamma = 4sV_\infty \sum_{n=1}^{\infty} nA_n \cos(n\theta).d\theta \qquad \textbf{(30)}$$

$$w_i = \frac{1}{4}\pi \int_{-s}^{+s} \frac{d\Gamma}{(y - y_i)} = V_\infty \sum_{n=1}^{\infty} \frac{nA_n \sin(n\theta)}{\sin(\theta)} \qquad \textbf{(31)}$$

$$C_l = a_o(\alpha_{2D} - \alpha_o) = \frac{2\Gamma}{V_\infty c} \qquad \textbf{(32)}$$

Where, a_0 is the section lift curve slope ($\frac{\partial C_l}{\partial \alpha}$), α_o is the zero lift angle and c is the section

$$\Gamma = \frac{1}{2} a_o V_\infty c(\alpha - \alpha_i + \theta_t - \alpha_o) \quad \textbf{(33)}$$

chord. Rearranging and substituting for the local angle of incidence.

Substituting for Γ and α_i in terms of the Fourier series approximations then a final boundary condition equation is obtained. The equation contains the unknown coefficients and the known geometric properties of the wing.

If a fixed number of coefficients (A_1, A_2, A_3, A_4.....A_N) is used then a set of simultaneous

$$\sum_{n=1}^{\infty} A_n \sin(n\theta)\left[\sin(\theta) + n\frac{a_o c}{8s}\right] = \frac{a_o c}{8s}\sin(\theta)(\alpha + \theta_t - \alpha_o) \quad \textbf{(34)}$$

linear equations will be obtained by applying the above equation at "N" span-wise locations. A cosine distribution of span-wise locations should be used to match the assumed wing loading distribution.

The number of coefficients used will determine the accuracy of the solution. If the wing loading is highly non-elliptical then a larger number of coefficients should be included. The solution for coefficients (A_1,A_2,A_3,A_4...A_N) is obtained by the reduction of the resulting matrix of equations. It should be noted that in cases were the wing loading is symmetric then even coefficients (A_2,A_4,A_6,....) will be zero and can be deleted from the calculation. The lift coefficient for the wing at a given angle of attack will be obtained by integrating the span-wise vortex distribution.

$$L = \rho V_\infty \int_{-s}^{+s} \Gamma dy \quad \textbf{(35)}$$

So that, $\mathbf{C_L = \pi . A_R . A_1}$, where $\mathbf{A_R}$ is wing aspect ratio. The down-wash velocity induced at any span location can be calculated once the strength of the wing loading is known. The variation in local flow angles can then be found.

$$D_i = \rho V_\infty \int_{-s}^{+s} \Gamma \sin(\alpha_i) dy \quad \textbf{(36)}$$

A consequence of this down-wash flow is that the direction of action of each section's lift vector is rotated relative to the free-stream direction. The local lift vectors are rotated backward and hence give rise to a lift induced drag. By integrating the component of section lift coefficient that acts parallel to the free-stream across the span, the induced drag coefficient can be found. So that, $\mathbf{C_{Di} = \pi . A_R . \Sigma (n A_n^2)}$

No real information about pitching moment coefficient can be deduced from lifting line theory since the lift distribution is collapsed to a single line along the 1/4 chord.

3.4.1 Special case of elliptical loading:

If the wing plan-form is elliptical, then it can be assumed that the wing load distribution is also a purely elliptical function.

$$\Gamma (y) = 4sV\infty A_1 \sin(\theta) = \Gamma_o \sin(\theta) \quad (37)$$

In this case a single general boundary condition equation results containing only one unknown, the vortex line strength at the wing root. The exact solution of this equation leads to the following simple answer for lift coefficient and induced drag coefficient.

$$\frac{\partial C_L}{\partial \alpha} = \frac{a_o}{\left(1 + \frac{a_o}{\pi AR}\right)} \quad (38)$$

$$C_{Di} = \frac{C_L^{\,2}}{\pi . AR} \quad (39)$$

$$\alpha_{o(2D)} = \alpha_{o(3D)}$$

Chapter : 04

MATHEMATICAL ANALYSIS

Before deriving the mathematical formula of thrust for the new propeller model, some assumptions have to be taken into consideration. Since this model is newly made and has not yet been measured in a large-scale project or made any model, so there might have been some inevitable shortcomings through the experimental research [15].

4.1 Assumptions

The principal assumptions which are supposed to be considered at first in order to ascertain the mathematical approach are as follows:

i. The propeller (belt drive) is considered as a revolving disc (actuator) ,

ii. The disc is fixed at its position when it rotates ,

iii. The surrounding water (fresh) around the disc is considered as an ideal fluid ,

iv. The flow upstream and downstream of the disc are taken as irrotational flow ,

v. The fluid is also taken as inviscid ,

vi. There are sudden pressure differences before and after the disc throughout the fluid along the direction of fluid flow ,

vii. There is a small portion of fluid on the propeller blade (aerofoil), which is considered as the control volume to calculate the thrust of that aerofoil and thereafter to measure it all over the propeller (belt drive) by successive integration,

viii. The aerofoil's pitch angle is let to be constant through the calculation; further scientific approach can be optimized by changing it according to the rules of hydrodynamics.

4.2 Derivation of the Equation for Thrust

The derivation of the equation for generated thrust starts with taking into consideration that, an aerofoil which is fitted on the belt drive rotates along with the moving belt as well as the propeller hub. The inviscid, irrotational fluid is surrounding the aerofoil, where it is one of the blade sections of a large blade.

If the thrust on the aerofoil is measured, then the thrust acting on the blade can be measured and hence the total thrust for the all blades (propeller) can also be measured. A conceptual schematic figure of the rotating aerofoil is given below:

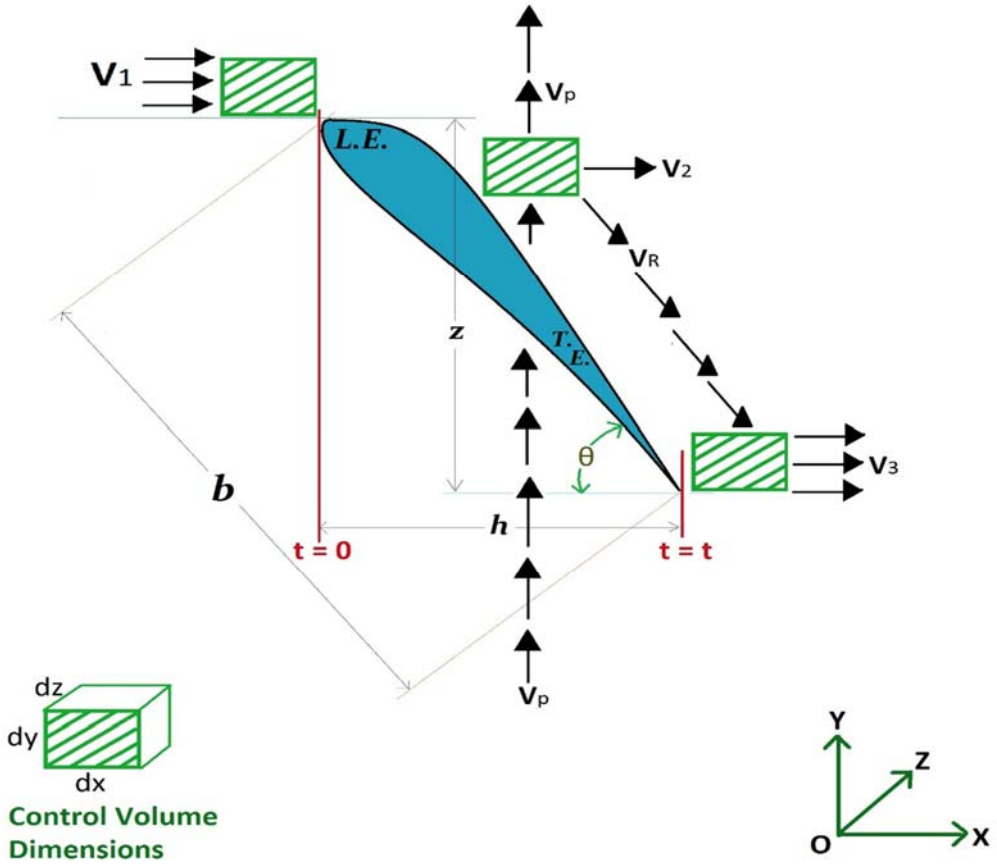

Figure 12: Fluid particle (control volume) flows over a blade section

As per the figure, let these below units be expressed in terms of thrust, that is:

Control volume dimensions (m) = **dx, dy, dz**

Density of fresh water (kgm^{-3}) = **ρ**

Propeller pitch angle ($radian$) = **θ**

Propeller chord length (m) = **b**

Propeller's rotational speed ($r.p.m.$) = $\mathbf{V_P}$

Axial velocity of water (ms^{-1}) = $\mathbf{V_1, V_2, V_3}$

Resultant velocity of control volume (ms^{-1}) = $\mathbf{V_R}$

Axial projected lengths of blade (m) = **h, z**

Thrust of propeller (N) = **T**

Total Area of propulsion (m^2) = **A**

Propeller radius from hub (m) = **R**

Radius of the hub (m) = **r**

Therefore, the derivation begins with,

At time, **t = 0**, initial momentum of the fluid flow = $\dot{\mathbf{m}}\mathbf{V_1}$

At time, **t = t**, final momentum of the fluid flow = $\dot{\mathbf{m}}\mathbf{V_R}$

Where, $\dot{\mathbf{m}}$ = mass flow rate per unit time,

$$\text{Or, } \dot{\mathbf{m}} = \rho.\left(\frac{dv}{dt}\right)$$

$$\text{Or, } \dot{\mathbf{m}} = \rho.\left(\frac{dx.dy.dz}{dt}\right) \tag{1}$$

So, after control volume have passed the trailing edge from the leading edge, change occurs in momentum in an instant time ***dt*** ,

$$d\dot{\mathbf{m}} = \dot{\mathbf{m}}(\mathbf{V_R} - \mathbf{V_1}) \tag{2}$$

When $\mathbf{t = 0}$, it can be assumed that, $\mathbf{V_2}$ and $\mathbf{V_1}$ has the same magnitude, or $\mathbf{V_2 = V_1}$ and thus, Equation (2) becomes,

$$\mathbf{d\dot{m} = \dot{m}(V_R - V_2)}$$

$$\text{Or, } \mathbf{d\dot{m} = \rho.}\left(\frac{dx\,.dy\,.dz}{dt}\right)\mathbf{.(V_R - V_2)} \tag{3}$$

In accordance with the law of momentum, thrust is equal to the change of momentum. Therefore,

$$\mathbf{d\dot{m} = dT = \rho.}\left(\frac{dx\,.dy\,.dz}{dt}\right)\mathbf{.(V_R - V_2)} \tag{4}$$

$$\text{Or, } \int_0^T dT = \mathbf{(\rho.}\,\frac{dz}{dt}\,\mathbf{)}\int_0^h\int_0^z \mathbf{(V_R - V_2).dx.dy} \tag{5}$$

Now, let us assume that, three velocity components are acting in such a way, that they make a right angled triangle and thus,

$$\mathbf{V_R} = \sqrt{\ }\,\mathbf{(V_p^2 + V_2^2)}$$

From the figure of the blade element geometry it is seen also,

$$\mathbf{b.\sin\theta = z} \text{ and } \mathbf{b.\cos\theta = h},$$

$$\mathbf{V_2 = V_R.\cos\theta} \text{ and } \mathbf{V_P = V_R.\sin\theta},$$

As it is reduced to two dimensional analysis and hence, $\mathbf{dz = 1}$ (say, it is unity)

Now, putting all those values above into Equation (5) and going through successive integration, what comes to light is:

$$\int_0^T dT = \mathbf{(}\,\frac{\rho.1}{dt}\,\mathbf{)}\int_0^h\int_0^z \mathbf{(V_R - V_R.\cos\theta)\,dx.dy}$$

$$\text{Or, } \mathbf{(T-0) =}\,\frac{\rho}{dt}\,\mathbf{.V_R.(1-\cos\theta)}\int_0^h\Big(\int_0^z \mathbf{dy}\Big)\mathbf{dx}$$

$$\text{Or, } \quad \mathbf{T = V_R.(1-\cos\theta)}\,\frac{\rho}{dt}\,\mathbf{.z.}\int_0^h \mathbf{dx}$$

$$\text{Or, } \mathbf{T = z.h.V_R.(1-\cos\theta).(} \frac{\rho}{dt} \mathbf{)} \qquad (6)$$

If, Equation (6) is expressed in terms of "$\mathbf{V_P}$" then, Equation (6) reduces to as follows:

$$\mathbf{T = z\,.\,h\,.\,(} \frac{\rho}{dt} \mathbf{).(}\frac{Vp}{\sin\theta}\mathbf{).(1-\cos\theta)}$$

$$\text{Or, } \mathbf{T = (\operatorname{cosec}\theta - \cot\theta).h.z.V_P.(} \frac{\rho}{dt} \mathbf{)} \qquad (7)$$

Now, putting the values of '**h**' and '**z**' into Equation (7) and hence,

$$\mathbf{T = (\operatorname{cosec}\theta - \cot\theta).b^2.\sin\theta.\cos\theta.V_P.(} \frac{\rho}{dt} \mathbf{)}$$

$$\text{Or, } \mathbf{T = (1-\cos\theta).b^2.\cos\theta.V_R.(} \frac{\rho}{dt} \mathbf{)} \qquad (8)$$

If the pitch angle remains unchanged or the propeller is fixed-blade system, then '**θ**' reduces into constant for a certain propeller system. Eventually, Equation (8) becomes as follows:

$$\mathbf{T = K\ .b^2.V_R.(} \frac{\rho}{dt} \mathbf{)} \qquad (9)$$

Where, $\mathbf{K = (1-\cos\theta).\cos\theta = 2\sin^2}\frac{\theta}{2}\mathbf{\,.\,(1-2\sin^2}\frac{\theta}{2}\mathbf{)}$ = Constant.

This is true only for two dimensional analyses.

4.3 Validation by Dimensional Analyses

For three dimensional analyses, Equation (9) should be slightly changed into its earlier form. The final equation of thrust for three dimensional analyses can be derived by linearizing Equation (9) with respect to '**dz**' & hence the equation reduces to:

$$\mathbf{T = K\ .b^3.V_R.(} \frac{\rho}{dt} \mathbf{)} \qquad (10)$$

Again, the conventional thrust equation for the propeller is:

$$\mathbf{T} = \frac{1}{2}.\mathbf{C_F}.\ \boldsymbol{\rho}.\ \mathbf{A}.\ \mathbf{V_R^2} \qquad (11)$$

Where, $\mathbf{C_F}$ = Coefficient of friction, $\mathbf{A}$ = Area of wet-surface.

It is known that, the dimension of units from Equation (11) and it is **[MLT $^{-2}$]**. Now, this research objective would be to compare the dimensional value of Equation (10) and this has been mathematically checked out below:

$$\mathbf{[T] = K\ .b^3.V_R.}\left(\frac{\rho}{dt}\right)$$

Or, **[T] = Constant . [Length]^3 . [Velocity] . [Density] . [Time]$^{-1}$**

Or, **[T] = [L]^3. [LT $^{-1}$] . [ML $^{-3}$]. [T]$^{-1}$**

Or, **[T] = [MLT $^{-2}$]** ; {similar as the **[Force]** following S.I. measurements}

This is most nearly visible as similar as the dimensional form of the conventional equation of thrust, delivered by the propeller in ship's propulsion.

Since, this derived mathematical expression, Equation (10) has the same dimensions as the conventional one; therefore this expression should also fulfill all the non-dimensional forms of thrust, velocity and moment. The non-dimensional terms [6] used to express the general performance characteristics are as follows [16]:

$$\text{Thrust coefficient, } K_T = \frac{T}{\rho n^2 D^4} \qquad (12)$$

$$\text{Torque coefficient, } K_Q = \frac{Q}{\rho n^2 D^5} \qquad (13)$$

$$\text{Advance coefficient, } J = \frac{V_a}{nD} \qquad (14)$$

In the next chapters, it will be shown how this pen and paper theory could be experimented through a physical model and therefore gathering data and building up a calculation based comparison from the help of ***"Iterative Average Theory"*** [17].

Chapter: 05

EXPERIMENTAL SETUP

The experiment, after mathematical prediction, was needed a physical evidence that could prove not only the authenticity but, for the scientific purposes, also efficiency as well. In order to setting up a workable mechanical device; different types of electronic individual equipment were assembled into one. Connecting one device with another, the model was set out for test run where the measurements went by, especially the Thrust vs. RPM, current consumption by the device, etc. An explanation about the functionality of the model is given afterwards in brief with the help of some necessary figures. It is followed, the upcoming part of this section would show the essential small electronic devices with their own figures, their description in a nutshell, the connectivity diagram and how it was managed to build some other things that were not as available or readymade as it seemed.

5.1 Electronic Modules

If the electrical devices are observed at a glance in a figure, then it will be much easier to describe about these parts one by one. The figure is demonstrating the six essential devices as follows:

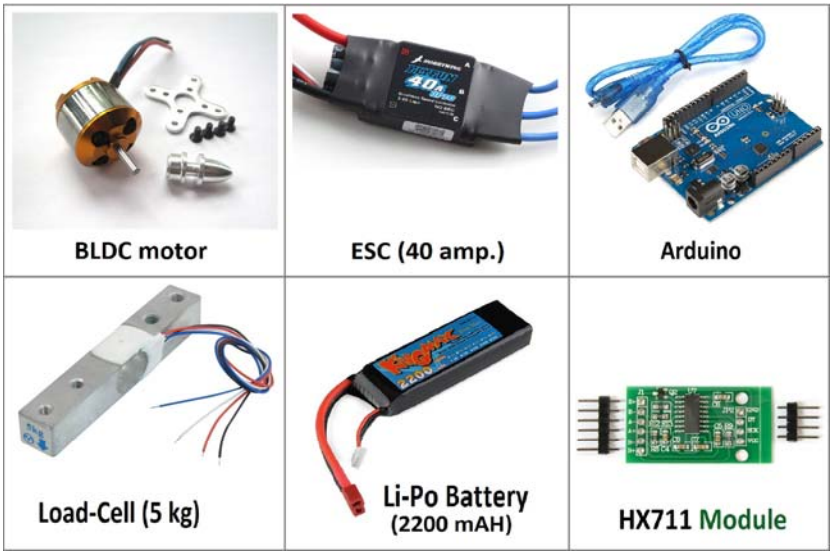

Figure 13: Electronic Modules for Experimental Setup

Now, a brief description has been given about the working principles of the above modules serially as the figure showed.

5.1.1 BLDC (Brushless Direct Current) Motor

The Brushless DC (BLDC) motor is the ideal choice for applications that require high reliability, high efficiency, and high power-to-volume ratio. Generally speaking, a BLDC motor is considered to be a high performance motor that is capable of providing large amounts of torque over a vast speed range. BLDC motors are a derivative of the most commonly used DC motor, the brushed DC motor, and they share the same torque and speed performance curve characteristics. The major difference between the two is the use of brushes. BLDC motors do not have brushes (hence the name "brushless DC") and must be electronically commutate. A figure is attached below:

BLDC motor

Figure 14: BLDC Motor

Another purpose for using that type of motor was that, the BLDC motor can be operated under water as it has no brush at all [18]. In this research, a particular BLDC motor was used to generate torques that was needed to calculate the thrust of the propeller. Basically, the motor acted as the propeller hub for the mounted belt drive. The motor (Model: A2212/ 13T/ 930KV) specifications were as follows:

Table 1: Technical Specification of BLDC Motor

No. Of cells needed	3 Li-Po (Lithium-Polymer)
RPM/V	930 KV
Max. efficiency current	4 - 10 A (>75%, = 80%)
No Load current / 10 V	0.5 A
Internal Resistance	90 mΩ
Current	0.5 A
Capacity	12A/ 60 s
Weight with cables	0.047 Kg

Max Efficiency	80%
Max Efficiency Current	4 - 10A (>75%)
No Load Current	0.5A @10V
Resistance	0.090 ohms
Max Current	13A for 60S
Max Watts	150W
Weight	52.7 g
Size	28 mm dia. *X* 28 mm bell length
Shaft Diameter	3.2 mm
Poles	8
Model Weight	300 - 800g
Max speed	210,000 rpm for 2 poles BLM

5.1.2 ESC (Electronic Speed Control) Circuit

An electronic speed control or ESC is an electronic circuit with the purpose to vary an electric motor's speed, its direction and possibly also to act as a dynamic brake. ESCs are often used on electrically powered radio controlled models, with the variety most often used for brushless motors essentially providing an electronically generated three-phase electric power low voltage source of energy for the motor.

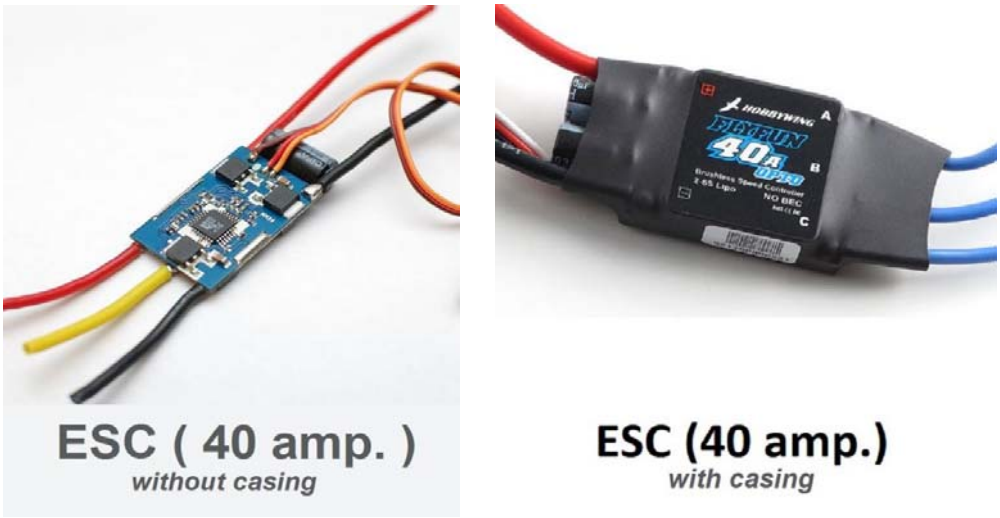

Figure 15: ESC (Electronic speed control)

ESCs designed for boats are by necessity waterproof. The watertight structure is significantly different from that of non-marine type ESCs, with a more packed air trapping enclosure. Thus arises the need to cool the motor and ESC effectively to prevent rapid failure. Most marine grade ESCs are cooled by circulated water run by the motor, or negative propeller vacuum near the drive shaft output. Like car ESCs, boat ESCs has braking and reverse capability.

5.1.3 Arduino (Uno)

The name "***Arduino***" comes from a bar in Ivrea, Italy, where some of the founders of the project used to meet. The bar was named after "***Arduin of Ivrea***", who was the king of Italy from 1002 to 1014. Arduino project was started in 2003 as a program for students at the Interaction Design Institute in Ivrea, Italy, aiming to provide a low-cost and easy way for novices and professionals to create devices that interact with their environment using sensors and actuators. This is an open source, computer hardware and software company, project, and user community that designs and manufactures micro-controller kits for building digital devices and interactive objects that can sense and control objects in the physical world. Arduino board designs use a variety of microprocessors and controllers. The boards are equipped with sets of digital and analog input/output (I/O) pins that may be interfaced to various expansion boards (shields) and other circuits.

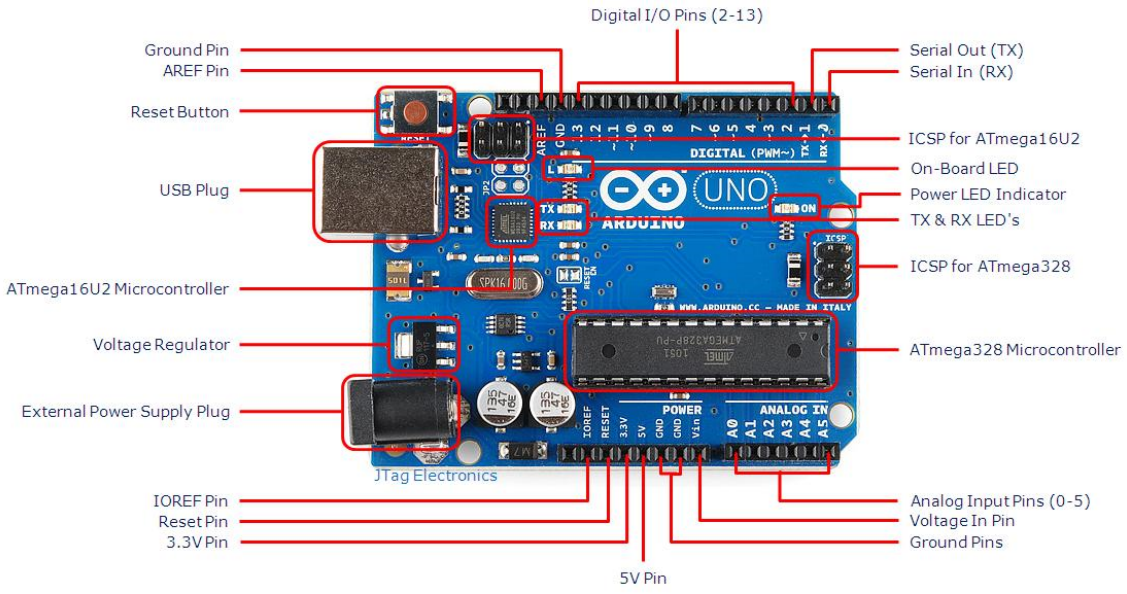

Figure 16: Arduino chipset Schematics (labeled)

The boards feature serial communications interfaces, including Universal Serial Bus (USB) on some models, which are also used for loading programs from personal computers. The micro-controllers are typically programmed using a dialect of features from the programming languages C and C++.

In addition to using traditional compiler tool-chains, the Arduino project provides an integrated development environment (IDE) based on the Processing language project.

The Arduino module has some basic features that have made it inevitable to use in the field of virtual sensing of the physical world, these are as follows:

Table 2: Technical Specifications of Arduino Chipset

Technical Specifications	
Input Voltage	7-12 V
Digital I/O Pins	20 (of which 6 provide PWM output)
PWM Output	6
PCB Size	53.4 x 68.6 mm
Weight	25 g
Product Code	A000066 (TH); A000073 (SMD)
Arduino (Micro-controller)	
Micro-controller	ATmega328
Architecture	AVR
Operating Voltage	5 V
Flash memory	32 KB of which 0.5 KB used by boot-loader
SRAM	2 KB
Clock Speed	16 MHz
Analog I/O Pins	6
EEPROM	1 KB
DC Current per I/O Pins	40 mA on I/O Pins; 50 mA on 3,3 V Pin

The Arduino Integrated Development Environment - or Arduino Software (IDE) - contains a text editor for writing code, a message area, a text console, a toolbar with buttons for common functions and a series of menus. It connects to the Arduino and Genuino hardware to upload programs and communicate with them. The Arduino Programmer is based on the Processing IDE and uses a variation of the C and C++ programming languages. To write basic codes in this IDE, one would need to learn some basic programming language syntax. Some important things to keep in mind when writing unique codes:

1. An Arduino program is called a "***Sketch***".

2. All code in an Arduino sketch is processed from top to bottom.

3. Arduino sketches are typically broken into five parts:

(a) The sketch usually starts with a header that explains what the sketch is doing, and who wrote it.

(b) Next, it usually defines global variables. Often, this is where constant names are given to the different Arduino pins.

(c) After the initial variables are set, the Arduino begins the setup routine. In the setup function, initial conditions of variables are set up when necessary, and run any preliminary code that it is only wanted to be run once. This is where serial communication is initiated, which is required for running the serial monitor.

(d) From the setup function, it goes to the loop routine. This is the main routine of the sketch. This is not only where your main code goes, but it will be executed over and over, so long as the sketch continues to run.

(e) Below the loop routine, there are often other functions listed. These functions are user-defined and only activated when called in the setup and loop routine.

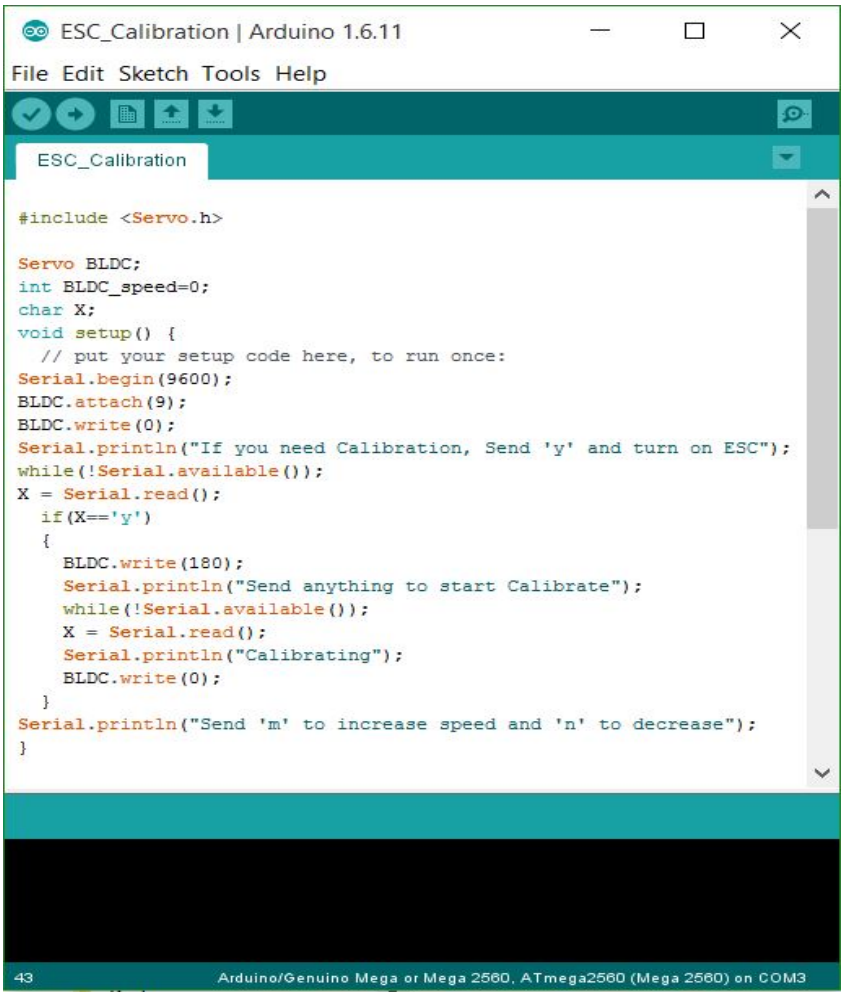

Figure 17: Interface of the Arduino programming editor (IDE)

4. All of that said, the only two parts of the sketch which are mandatory are the *"**Setup**"* and *"**Loop**"* routines.

5. Code must be written in the Arduino Language, which is roughly based on **C**.

6. Almost all statements written in the Arduino language must end with a "**;**"

7. Conditionals (such as if statements and for loops) do not need a "**;**"

8. Conditionals have their own rules and can be found under ***"Control Structures"*** on the Arduino Language Library.

Presumably, Arduino is the main control unit for the electronic module [19] of the experimental device or in other words, this the central processing zone of enormous data from the sensors, in a small scale measurement process.

5.1.4 Load Cell (5 Kg)

A load cell is a force sensing module - a carefully designed metal structure, with small elements called strain gauges mounted in precise locations on the structure. Load cells are designed to measure a specific force, and ignore other forces being applied. The electrical signal output by the load cell is very small and requires specialized amplification. Fortunately, the "***1046 Phidget Bridge***" will perform all the amplification and measurement of the electrical output [20].

Load cells are designed to measure force in one direction. They will often measure force in other directions, but the sensor sensitivity will be different, since parts of the load cell operating under compression are now in tension, and vice versa. There are mainly 3 types of load cell:

a) **Single point load cell,**
b) **Button load cell,**
c) **S-type load cell.**

It had been used the "**Class-(a)**" load cell from above for the experimental research. It would likely to be described a little about single point load cell with necessary figures.

a) Single-Point Load Cell

This Single Point Load Cell is used in small jewelry scales and kitchen scales. It's mounted by bolting down the end of the load cell where the wires are attached, and applying force on the other end in the direction of the arrow. Where the force is applied is not critical, as this load cell measures a shearing effect on the beam, not the bending of the beam. If you mount a small platform on the load cell, as would be done in a small scale, this load cell provides accurate readings regardless of the position of the load on the platform.

A single-point load cell. Applying force to one end creates stress in the bar, causing the strain gauge encased in the white plastic to flex.

Figure 18: load cell

It was chosen to use this type of load cell within range of 5 Kg thrust measuring capacity. This load cell has these unique features in itself:

Table 3: Technical Specifications of Load cell

Mechanical Specifications	
Housing Material	Aluminum Alloy
Load Cell Type	Strain Gauge
Capacity	5kg
Dimensions	55.25x12.7x12.7mm
Mounting Holes	M5 (Screw Size)
Cable Length	550mm
Cable Size	30 AWG (0.2mm)
Cable - no. of leads	4
Electrical Specifications	
Precision	0.05%
Rated Output	1.0±0.15 mv/V
Hysteresis	0.05% FS
Non-Repeatability	0.05% FS
Temperature Effect on Zero (per 10°C)	0.05% FS
Temperature Effect on Span (per 10°C)	0.05% FS
Zero Balance	±1.5% FS
Input Impedance	1130±10 Ohm
Output Impedance	1000±10 Ohm
Insulation Resistance (Under 50VDC)	≥5000 MOhm
Excitation Voltage	5 VDC
Compensated Temperature Range	-10 to ~+40°C
Operating Temperature Range	-20 to ~+55°C
Safe Overload	120% Capacity
Ultimate Overload	150% Capacity

5.1.5 Li-Po (Lithium-Polymer) Battery

Lithium Polymer batteries (henceforth referred to as "**LiPo**" batteries), are a newer type of battery now used in many consumer electronics devices. They have been gaining in popularity in the radio control industry over the last few years, and are now the most popular choice for anyone looking for long run times and high power.

Just as with other lithium-ion cells, **LiPo** works on the principle of intercalation and deintercalation of lithium ions from a positive electrode material and a negative electrode material, with the liquid electrolyte providing a conductive medium. To prevent the electrodes from touching each other directly, a micro-porous separator is in between which allows only the ions and not the electrode particles to migrate from one side to the other.

LiPo batteries offer three main advantages over the common Nickel-Metal Hydride (NiMH) or Nickel Cadmium (NiCd) batteries:

a. LiPo batteries are much lighter weight, and can be made in almost any size or shape.

b. LiPo batteries offer much higher capacities, allowing them to hold much more power.

c. LiPo batteries offer much higher discharge rates, meaning they pack more punch.

But, just as a coin has two sides, there are some drawbacks to LiPo batteries as well.

a) LiPo batteries have a shorter lifespan than NiMH/NiCd batteries. LiPos average only 300–400 cycles.

Figure 19: Litheum Polymer Battery

b) The sensitive chemistry of the batteries can lead to fire if the battery gets punctured and vents into the air.

c) LiPo batteries need special care in the way they are charged, discharged, and stored. The required equipment can be expensive.

Considering these features over all, what was used for this device's power source has these features below:

2200mAh, 3S, 12 V, 30C LiPo

i. Integrated LED indicator allows you to check state of charge at the push of a button.

ii. Powerful 40C continuous discharge rating to deliver excellent performance and longevity.

iii. 3C maximum charge rate for quick and safe recharging in as little as 20 minutes or less.

iv. Available in a variety of capacities and cell counts that are perfect for almost any application.

v. Equipped with balancing leads and a JST-XH connector compatible with most balancers and balancing chargers.

vi. No soldering required, equipped with an E-flite EC3 connector on the main power leads.

5.1.6 HX711 Module (The Amplifier)

Based on *Avia Semiconductor*'s patented technology, HX711 is a precision 24-bit analog to digital converter (ADC) designed for weigh scales and industrial control applications to interface directly with a bridge sensor.

The Load Cell Amplifier and ADC Module is a small breakout board for the HX711 IC that allowed us to easily read load cells to measure weight. By connecting the module to the micro-controller (Arduino) it was set up to read the changes in the resistance of the load cell and with some calibration, been able to get very accurate weight measurements. This might be handy for creating unique or new industrial scale, process control, or simple presence detection.

The HX711 uses a two wire interface (Clock and Data) for communication whereas; the load cells use a four wire wheat-stone bridge to connect to the HX711. These are commonly colored RED, BLK, WHT, GRN, and YLW. Each color corresponds to the conventional color coding of load cells:

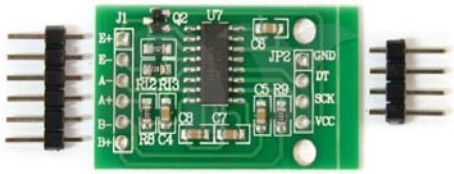

HX711 Module

Figure 20:HX711 Module

- Red (Excitation+ or VCC)
- Black (Excitation- or GND)
- White (Amplifier+, Signal+, or Output+)
- Green (A-, S-, or O-)
- Yellow (Shield)

This module is actually nothing but an amplifier which amplifies signals from the load cell's weight reading without calibration or without calibration as it is programed to,

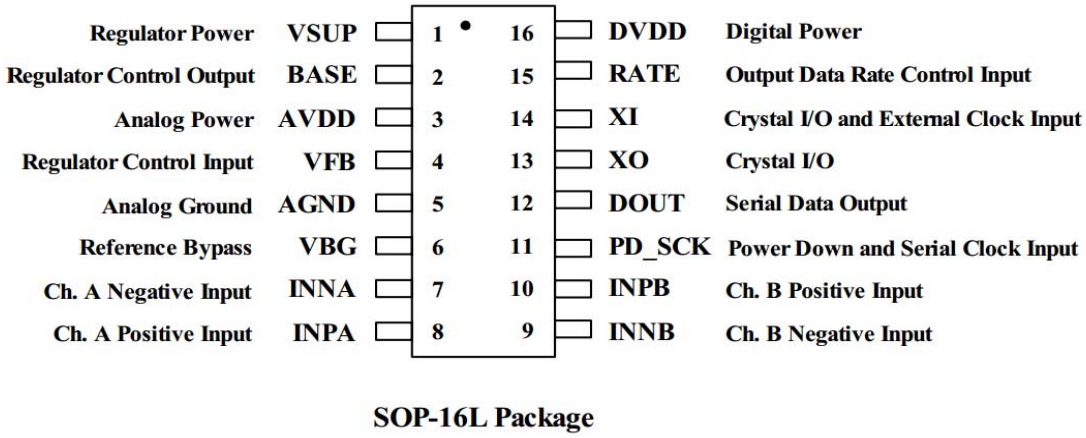

SOP-16L Package

Figure 21: Pin Descriptions of HX711 Module

Depending on the different variable functions at its 16 individual pins, the readings are extracted from the load cell through these pins. These pins are of special set of purposes.

5.2 Connectivity Arrangements

Arranging all the separate modules along with one another in a harmony as the device could work was the actual challenge to us. As because, the new modules were not tested before so there might be any corrupted data error or mechanical mishap. Nevertheless, the modules went not only good but also in a harmony while the data was being extracted through the thrust measurement process.

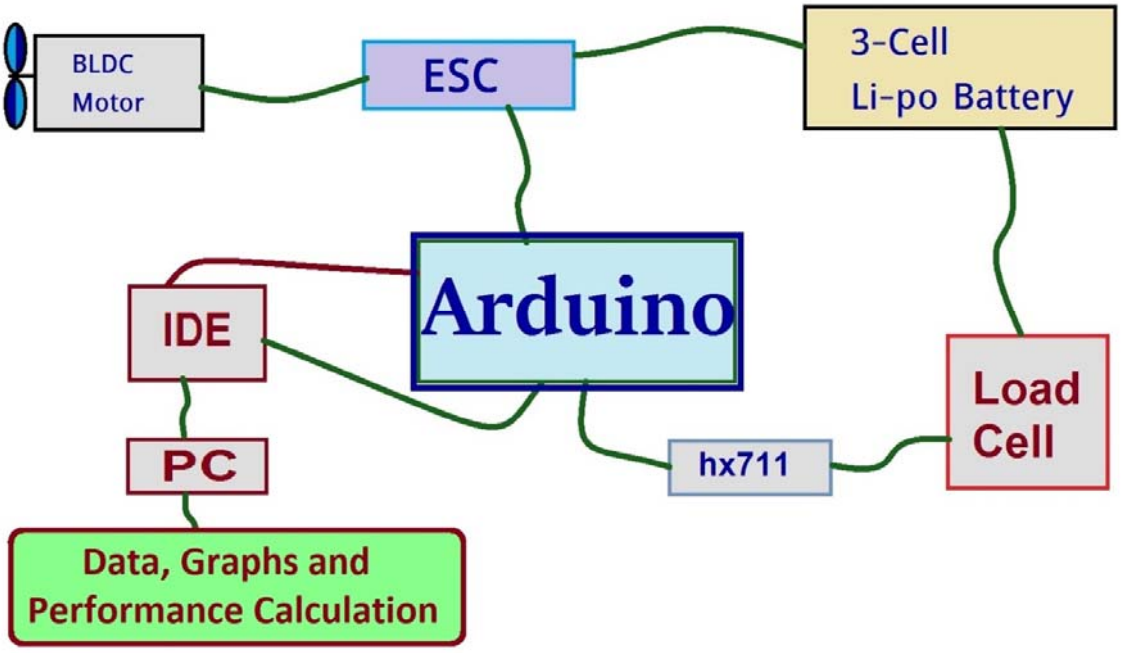

Figure 22: Connectivity Diagram of Different Modules

At first, the 3-cell LiPo battery was taken to the charger to be charged fully before being operational. Then it was soldered so that different modules into one another's ports or plugs. In example; ESC is connected with both the BLDC motor (propeller hub) and with the Arduino. Load cell was connected with its signal amplifier HX711 module and this amplifier went straight to Arduino also. After being fully charged, the 3-cell LiPo battery was connected to the ESC and hence, the BLDC motor rotated under the micro-controller program.

5.3 Propeller Blades

The intended propeller which are of different design and unorthodox mechanical function due to its particular reason, that is why, it was to design the outline and the concept of the propeller in 3-D CAD software (Rhinoceros) and then the design was saved in ***STL** (**stereo-lithography**) or, ***OBJ** (**object**) format. After that, the propeller blades were printed through a 3-D printer and thus the required blades were made as it was mentioned earlier. Concepts, design output and printed versions are given below.

5.3.1 Conceptual Output

The conceptual design was drawn in Rhinoceros (3-D) and the outputs were in "shaded" view mode as like as below:

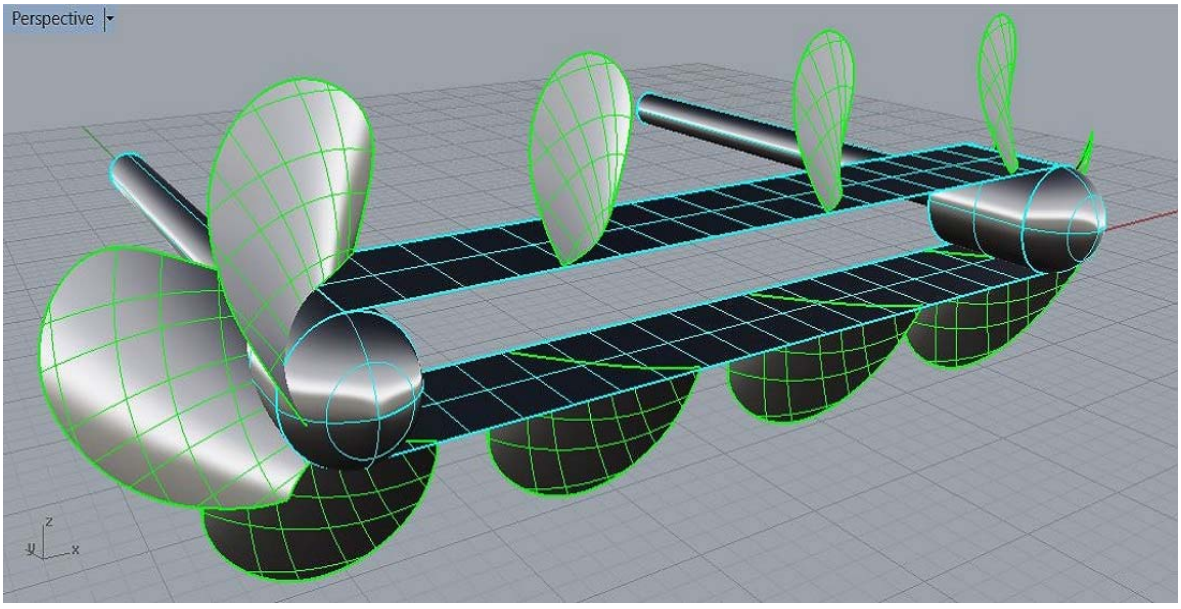

Figure 23: 3D Output of Coupled Propeller (Perspective View)

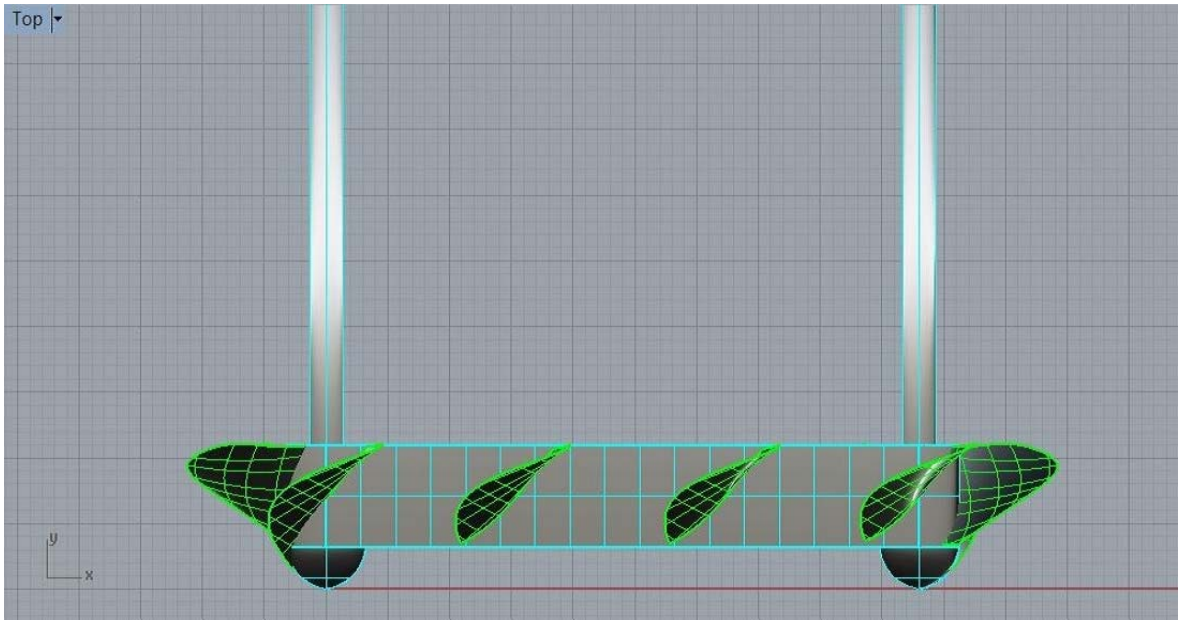

Figure 24: 3D Output of Coupled Propeller (Top View)

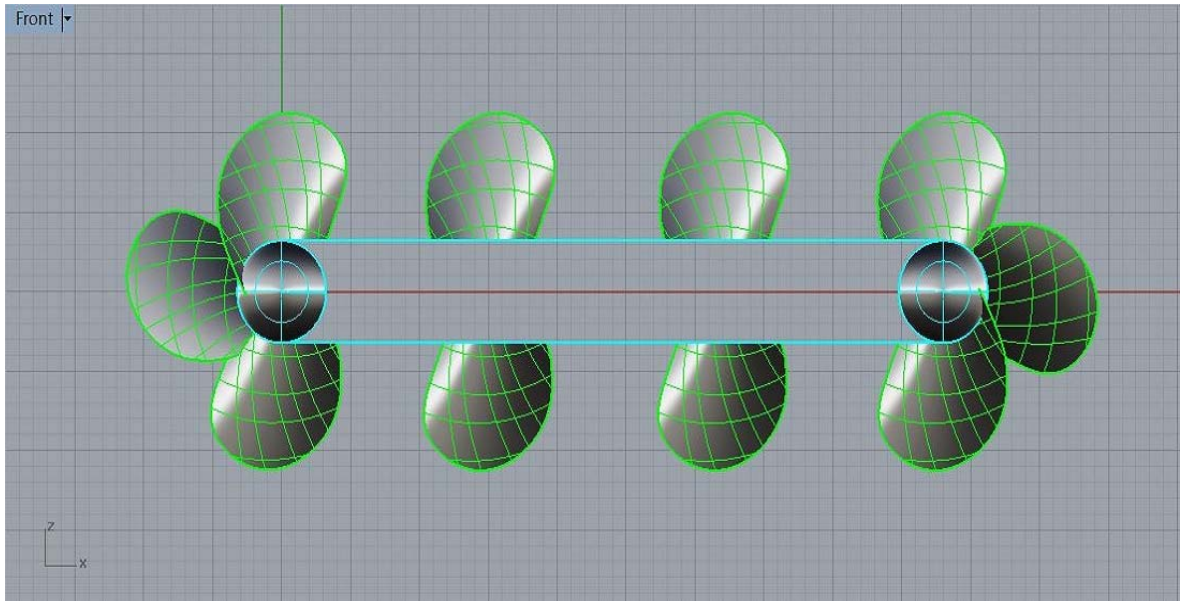

Figure 25: 3D Output of Coupled Propeller (Front View)

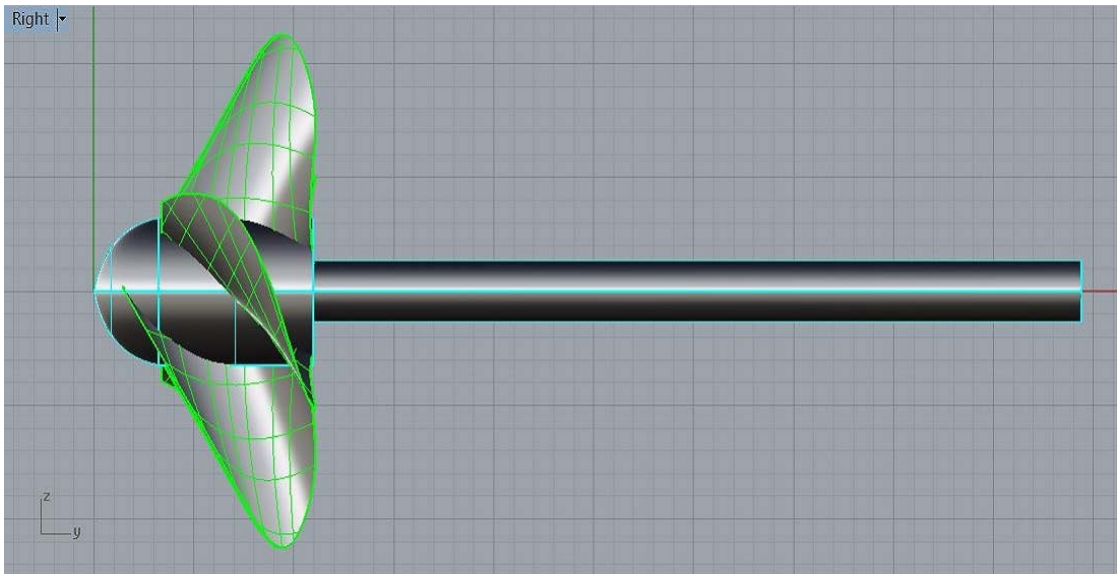

Figure 26: 3D Output of Coupled Propeller (Right View)

5.3.2 Object File (Printable Output)

Once the design was finalized, the object oriented design or the 3-D output had been designed over Rhinoceros and then it was printed as a solid mesh volume without any naked edges and hence we got:

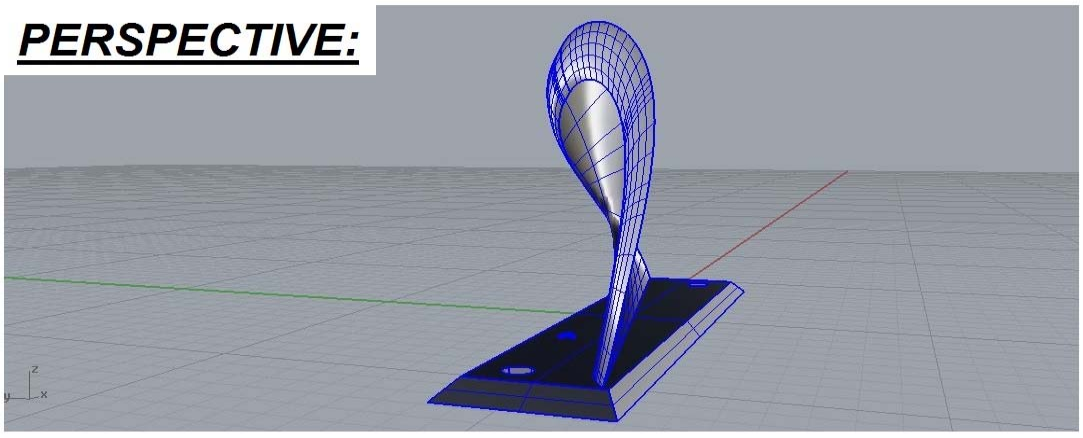

Figure 27: 3D Output of the Elemental Propeller Blade (Perspective view)

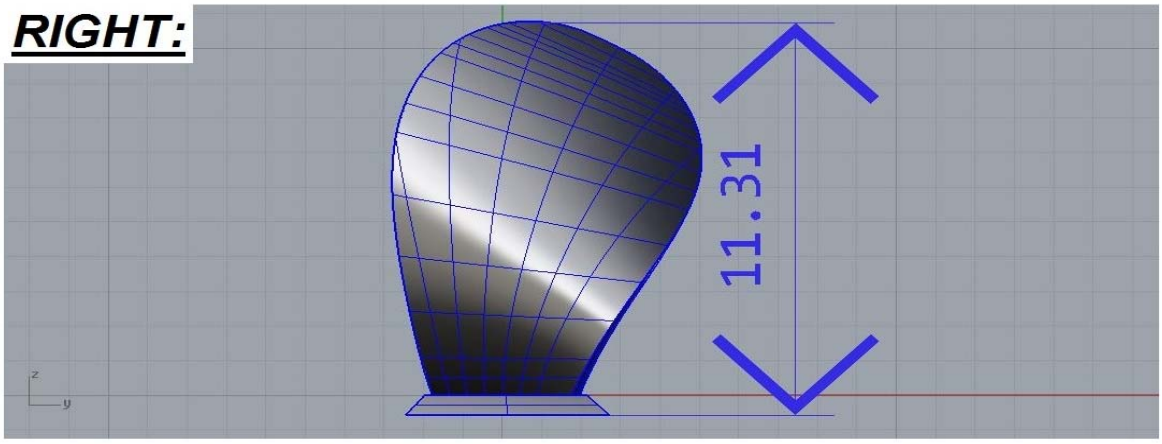

Figure 28: 3D Output of the Elemental Propeller Blade (Right view)

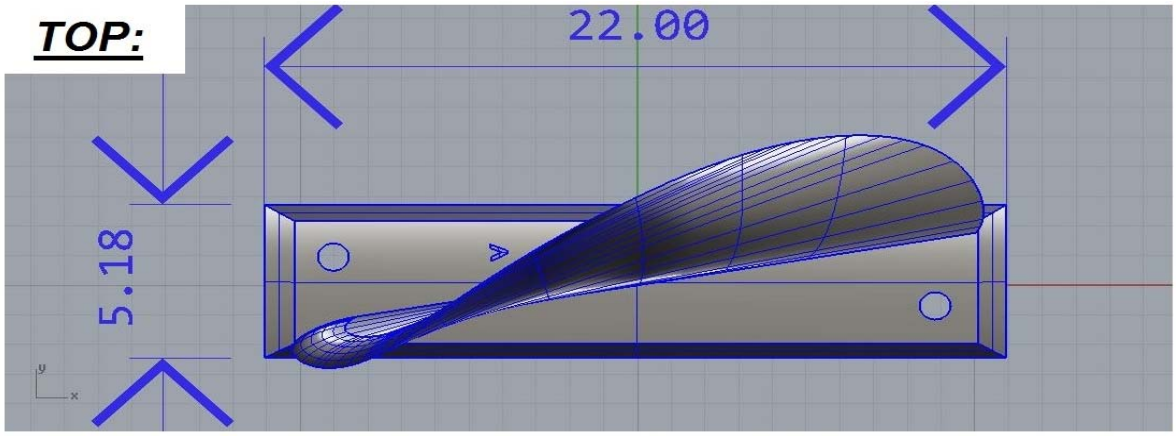

Figure 29: 3D Output of the Elemental Propeller Blade (Top view)

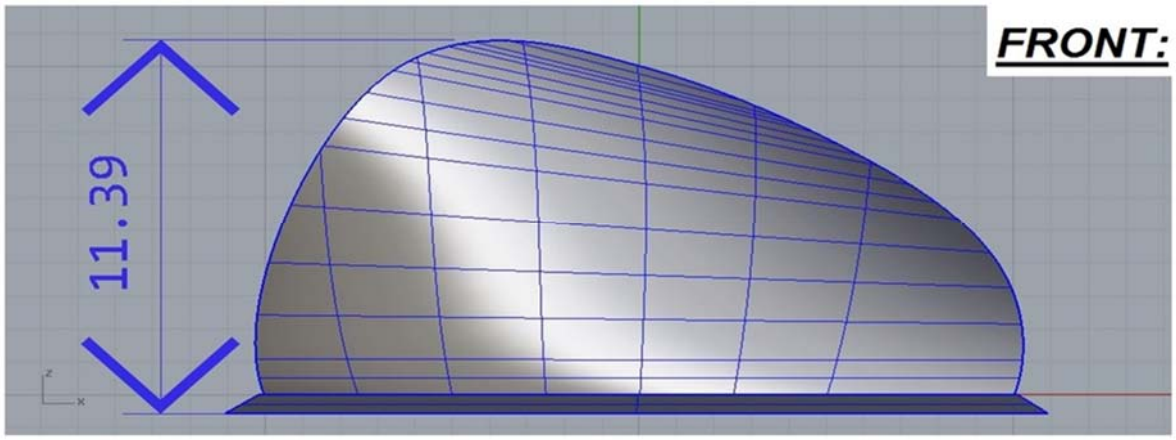

Figure 30: 3D Output of the Elemental Propeller blade (Front view)

5.3.3 Printed Blades (Elemental Unit of Propeller)

The blades were printed with Poly Vinyl Chloride (PVC) plastics and the total number of the blades that had been used for the experimental purpose was 10 (ten). The unit systems for the dimensions of the blades were of millimeter.

3-D Printed propeller blades (Total 10)

Figure 31: 3D Printed Propeller Blades

Some features of the 3D-printed propellers were:

i. Dimension: 22 **X** 5.2 **X** 11.4 (mm)

ii. Free surface area: 267 mm^2

iii. Epoxy raisin or super glue helped the blades to be fitted over the urethane belt surface.

iv. Blades are sewed with the belt surface for additional strengthening purpose.

v. Operational Length of the Belt is 202 mm.

5.4 Urethane Belt Drive

Urethane round belts are ideal for custom made conveyor applications and most other light to medium duty applications. This can be joined at the ends to create a custom belt by simply melting the tips of the material and sticking them evenly to one another until they cool (thermal cure process) down. Regarding the project, a piece of urethane belt is used for the propeller blades as the dynamic link between two propeller hubs.

Figure 32:Polyurethane Belts (Ring Type)

Propeller blades are attached on a piece of this type of belt. Specifications of which was used in this project are given as follows:

Table 4: Technical Specifications of urethane Belts

Technical Specification	
Peripheral Length	202 mm
Span	20 mm
Thickness	2 mm
Hardness	90±5 Shore A
Weight	10±2 g
Temperature	- 40 to 204℃

By using epoxy resin with hardener (1:1 ratio), propeller blades were attached on the outer surface of the belt drive. After attaching the blades, this belt was mounted on to the two propeller hubs. Therefore, in the next chapter, authenticity will be investigated of the derived thrust equation on the basis of these all mechanical set up.

5.5 Assembled Modules in a Glimpse

When all modules mentioned earlier in this thesis, were connected as a whole of a unique mechanical setup, had been ready for being operational for the experiment. All modules were separately mounted on wooden ply boards of different dimensions and thickness in terms of necessity and suitability. After all things got done, below images could specify how it looks like:

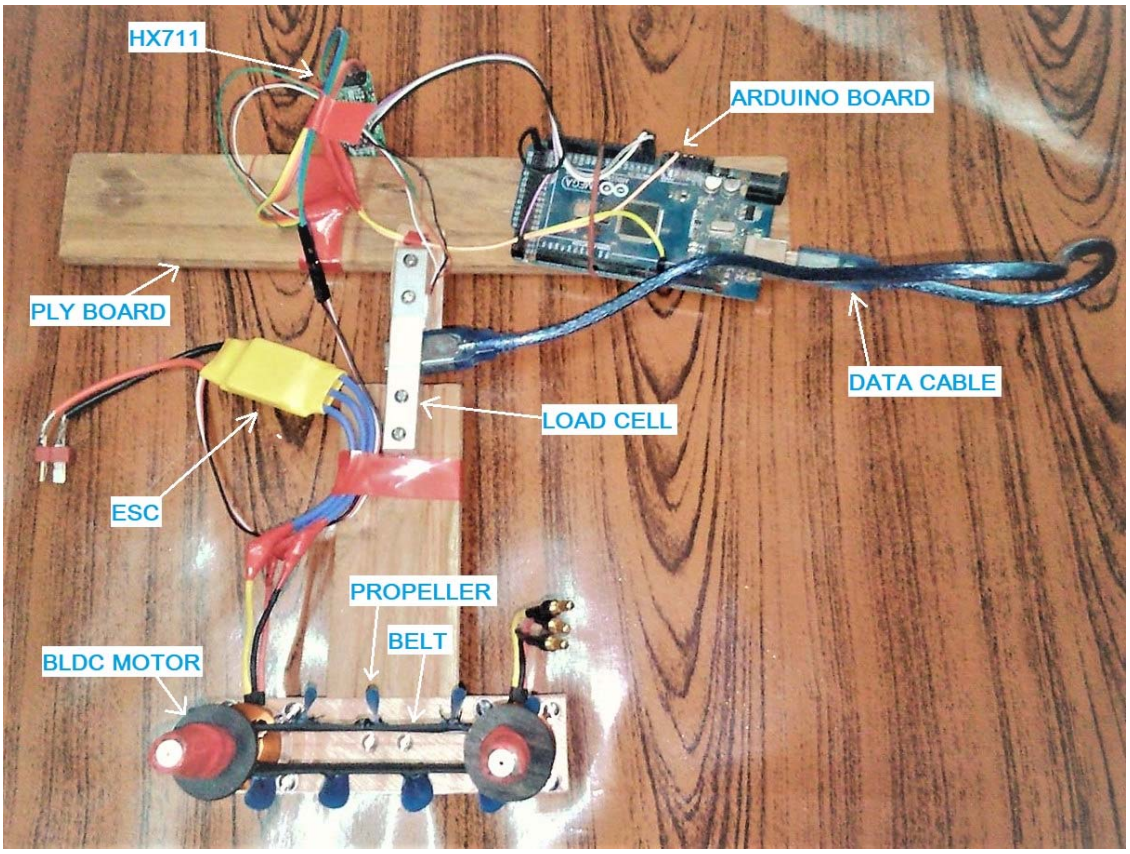

Figure 33: Modules Assembly

For the purpose of assembly on ply board, bolts and nuts had been used that were of 03 mm nominal diameter. In the above picture, one BLDC motor is seen without any connection, which was remained in that way as because it was not experimented that the thrust produced by twin screw propulsion system. All the modules were fixed in their positions and the combination of parts as well as wirings were held by scotch tapes. This ply board's lay out

were designed as like as it seems a **'T'** (tee) joint linking through the load cell with two bolts at **FLANGE** of the **'T'** and other two bolts at **WEB** of that **'T'**.

This sort of set up would make the load cell bend and hence estimate thrusts due to propulsion. Before putting this system down into the water (i.e. longitudinal basin or slender tank) these all items (except BLDC motor) had to be water tight for the sake of safety and accidents. Thick plastic polythene sheets were used to wrap up the exposed areas.

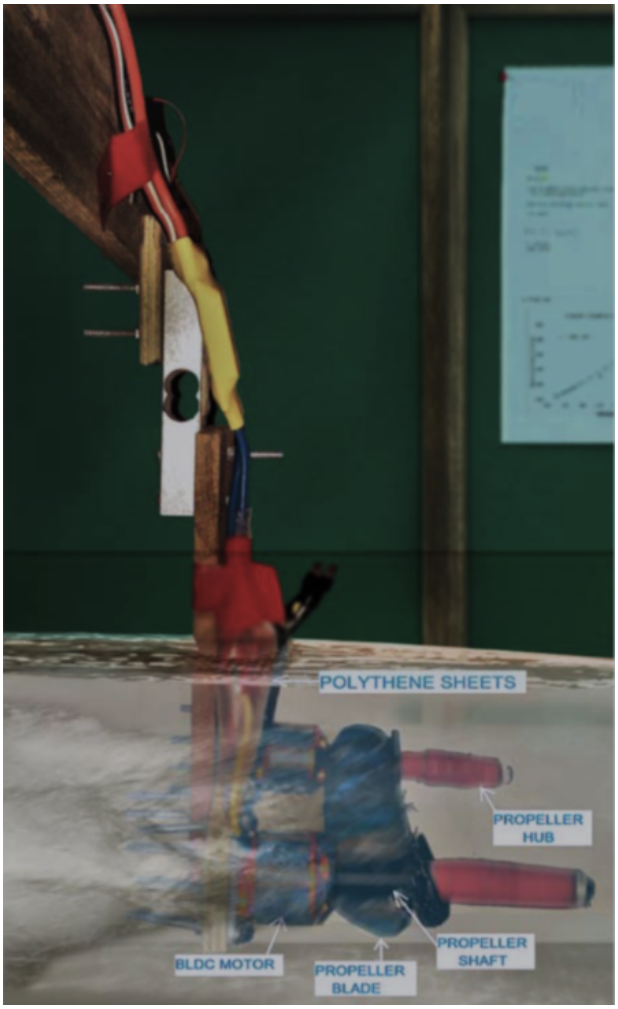

Figure 34: Propellers Underwater (Tank Test)

Arduino board and HX711 module were fixed on **FLANGE** without any metal bolts as because it may cause damages to the sophisticated integrated circuits (IC) on all over these two chips. So that, these two modules were fitted with the help of silicone made elastic girders

5.6 The “Sketch” for Thrust Estimation

A coding platform was necessary for controlling the connected modules in different aspects after each module had been connected into the Arduino chip. Basic syntax and logics were used in order to create the sketch in the Arduino along with the purpose of calibration for the load cell. Screenshots of the codes which were used to build this project are given below in terms of chronological serial:

5.6.1 ESC Calibration Codes

Figure 35: Source Code for ESC Calibration

5.6.2 HX711 Module Calibration Code

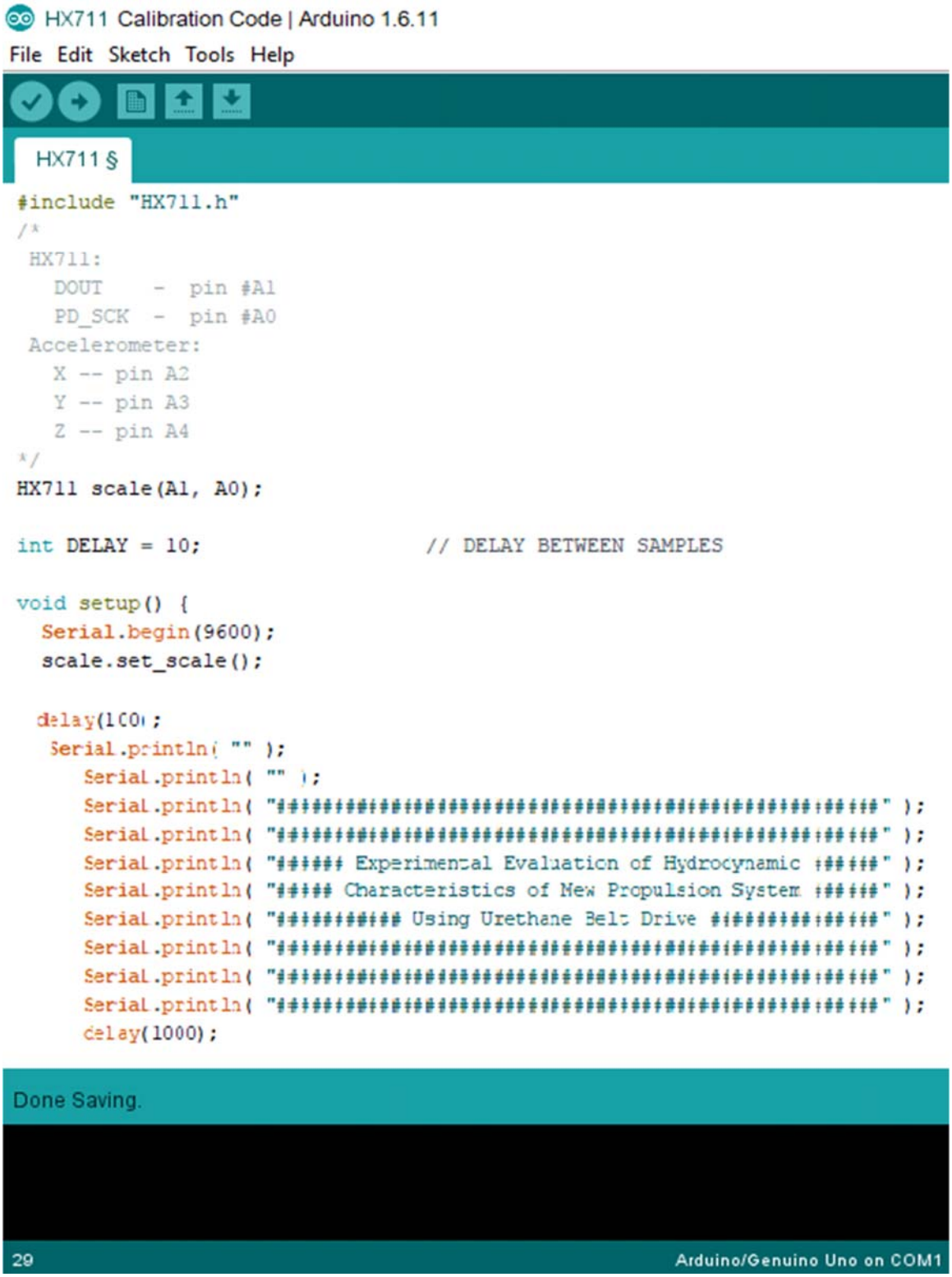

Figure : 36 Source Code for HX711 Calibration – page 1

Figure : 37 Source Code for HX711 Calibration – page 2

Figure : 38 Source Code for HX711 Calibration – page 3

Figure : 39 Source Code for HX711 Calibration – page 4

Figure : 40 Source Code for HX711 Calibration – page 5

Figure : 41 Source Code for HX711 Calibration – page 6

5.6.3 BLDC Motor Calibration Codes

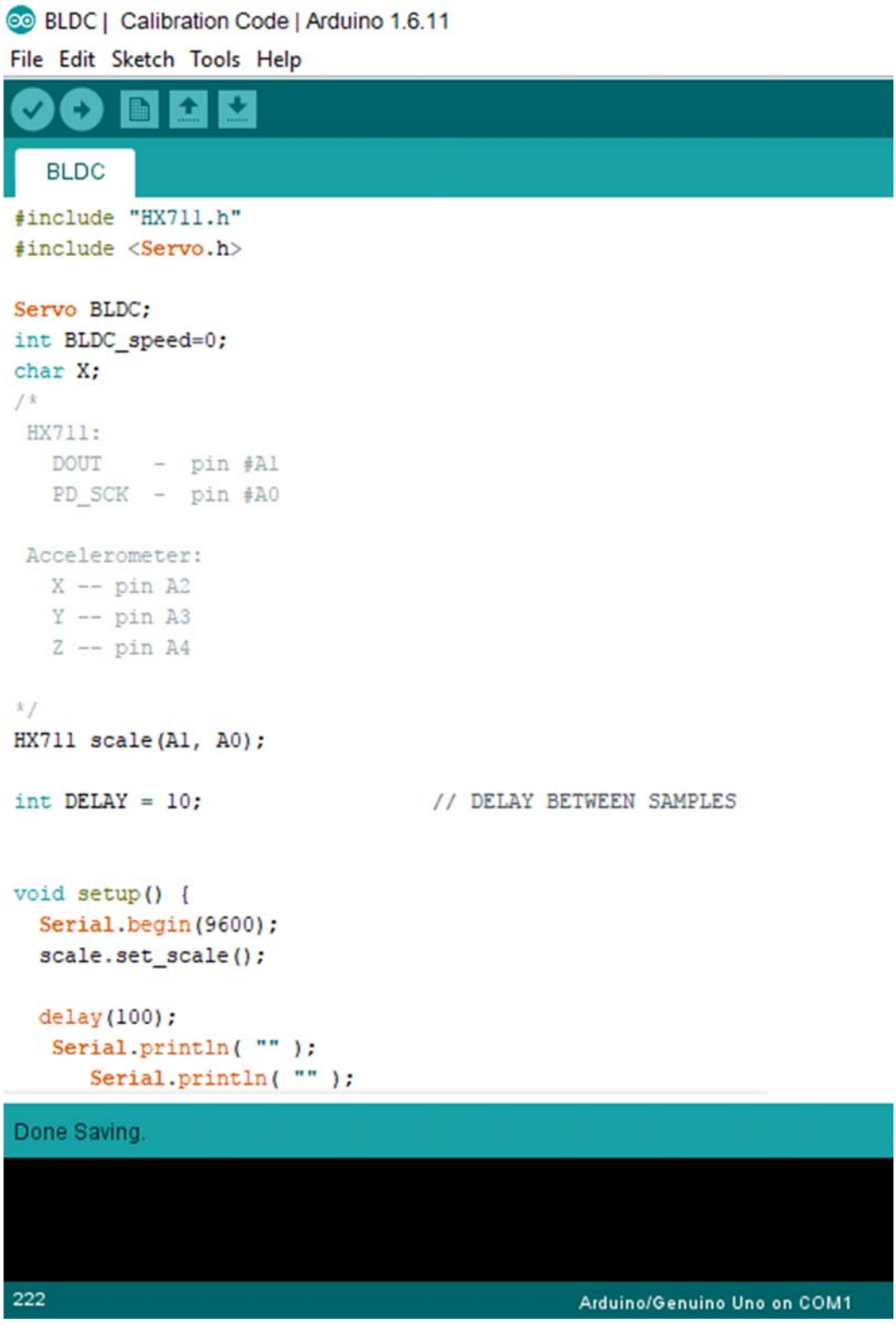

Figure : 42 Source Code for BLDC Motor Calibration – page 1

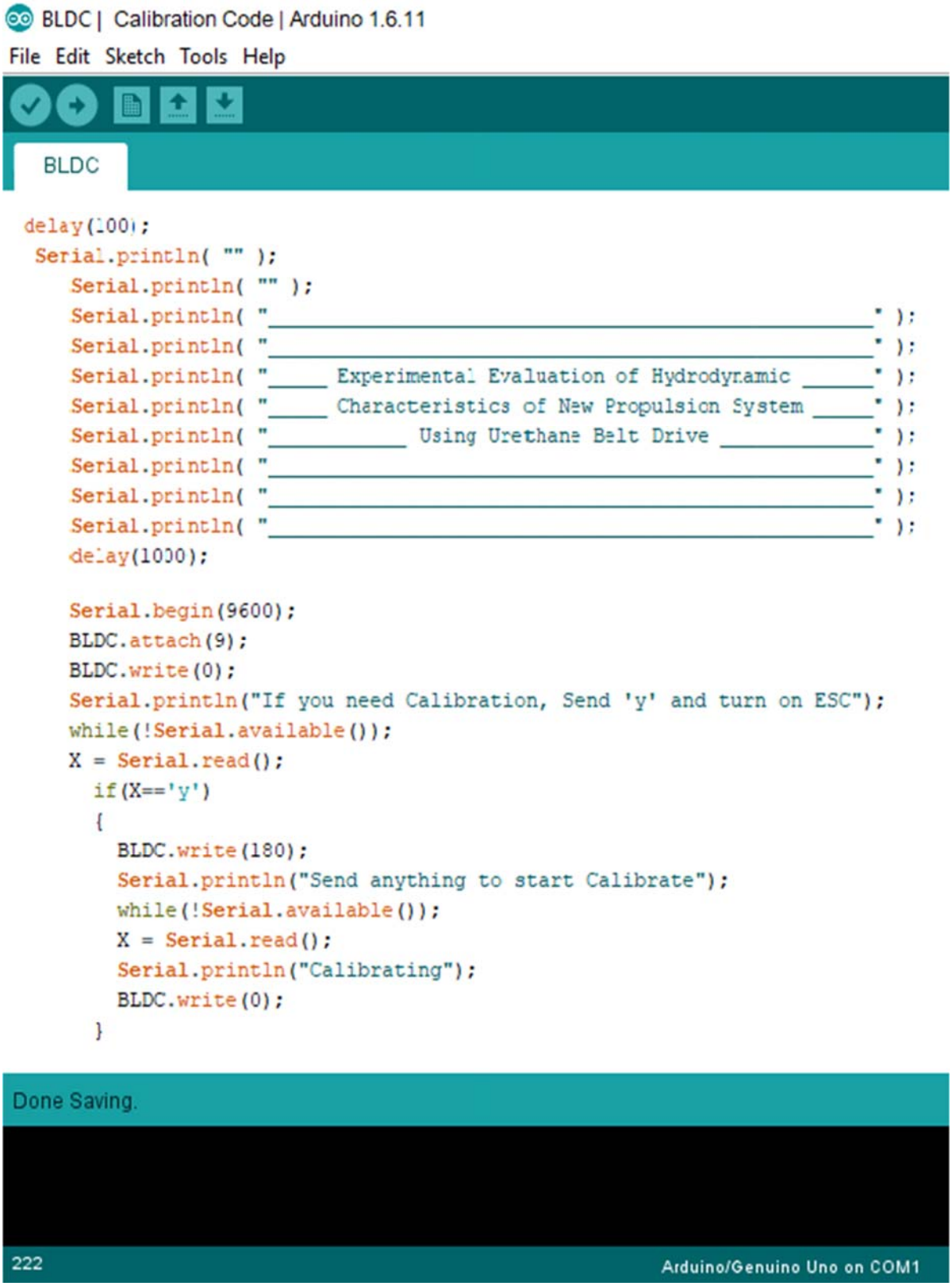

Figure : 43 Source Code for BLDC Motor Calibration – page 2

Figure : 44 Source Code for BLDC Motor Calibration – page 3

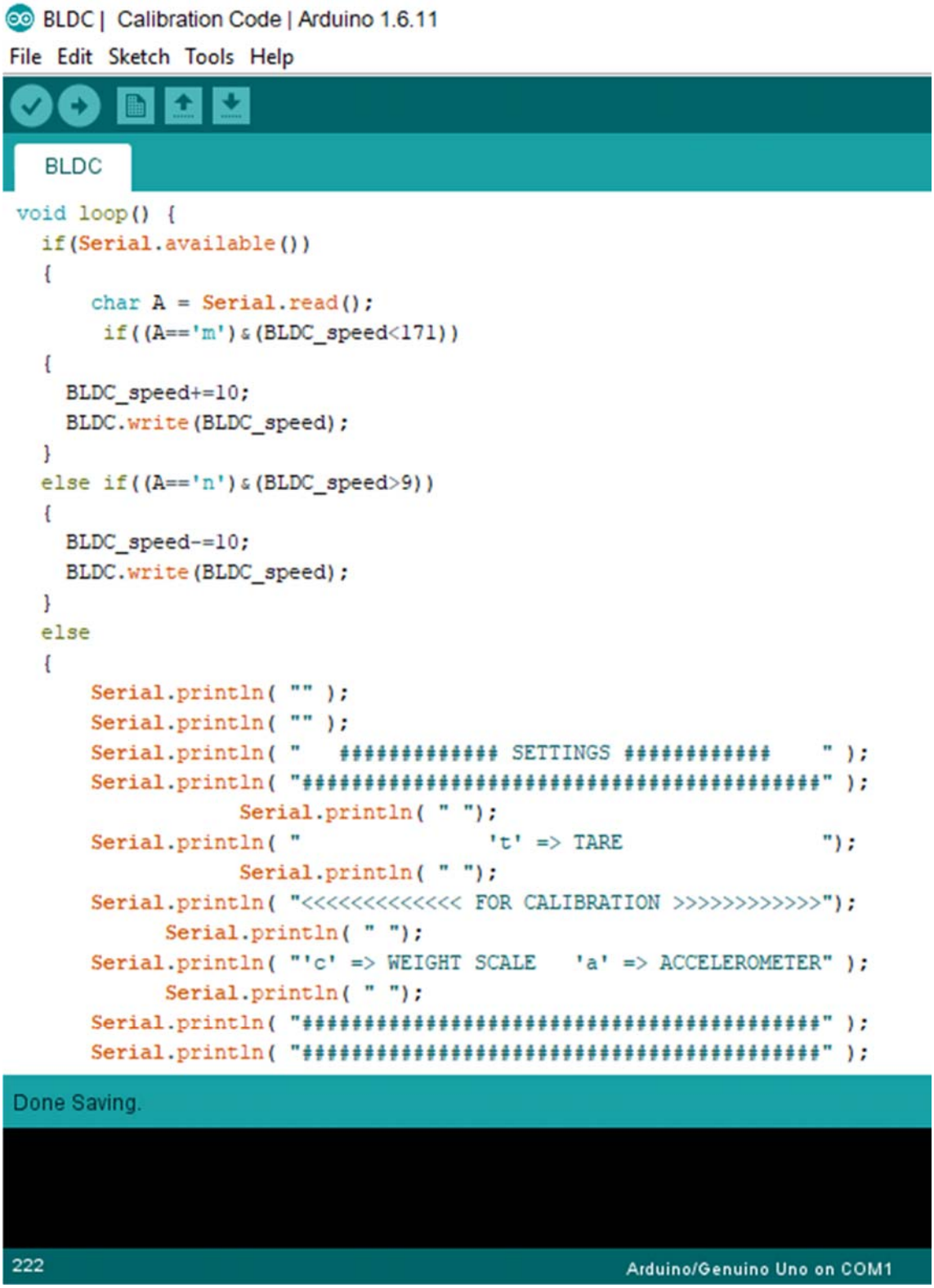

Figure : 45 Source Code for BLDC Motor Calibration – page 4

Figure : 46 Source Code for BLDC Motor Calibration – page 5

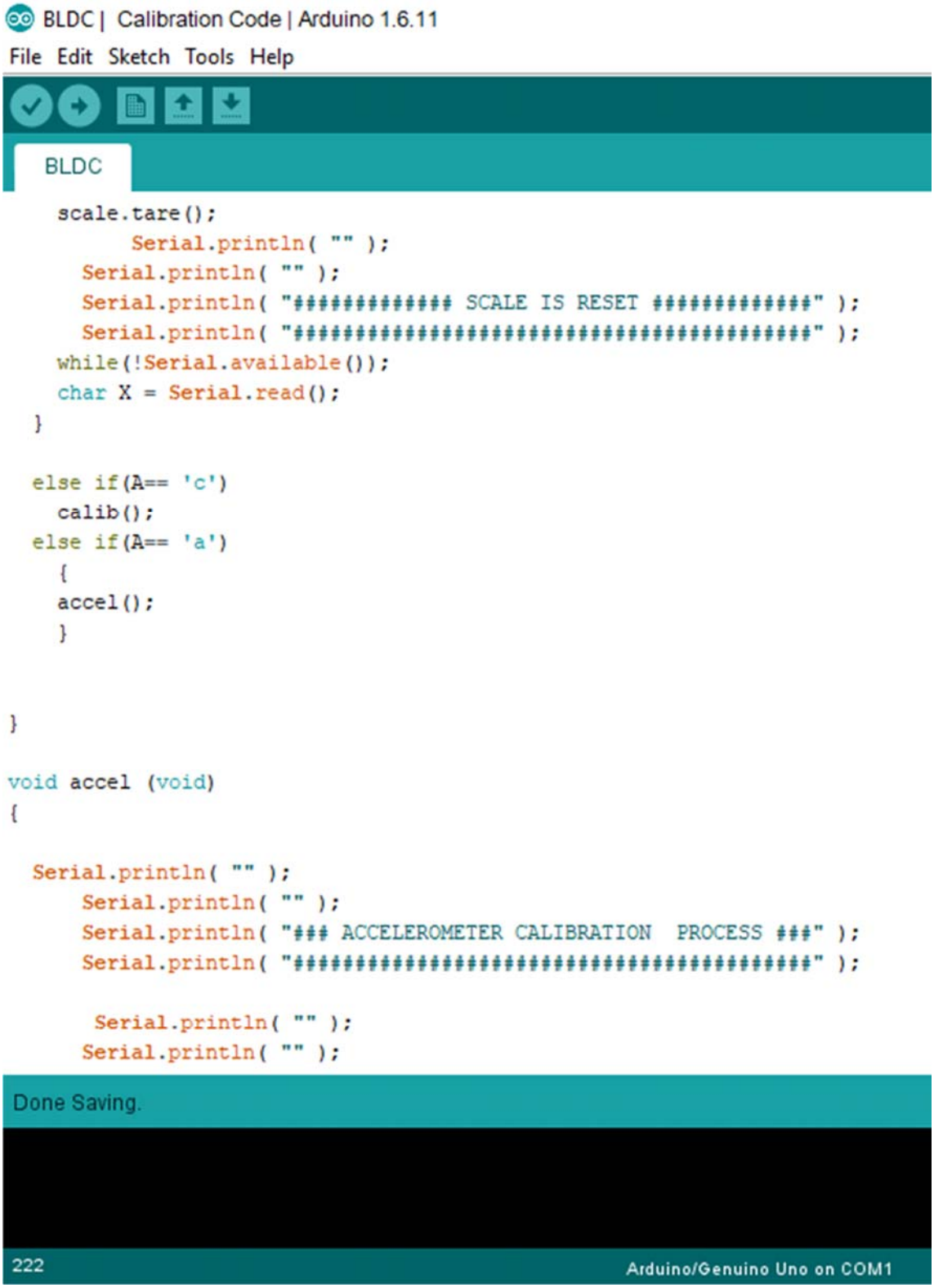

Figure : 47 Source Code for BLDC Motor Calibration – page 6

Figure : 48 Source Code for BLDC Motor Calibration – page 7

Figure : 49 Source Code for BLDC Motor Calibration – page 8

Chapter : 06

RESULTS AND DISCUSSION

6.1 Data and Results validation

All calculations that went through this chapter were based on the data output from mechanical (load cell) set up. The results obtained from Arduino setup can be affected by some atmospheric or electrical errors and uncertainties, such as the model errors and uncertainties, discretization (numerical) errors, iteration (convergence) errors, application uncertainties, user errors and code errors. Therefore, the results from the experimental set up for coupled-screw propeller will be compared with experimental data ran by the same mechanical set up for single screw propeller. This is how the comparative analyses might be counted as much as error free as because the same errors were in both process and omitted each other thereby.

6.2 Data Obtaining Methodology

Regarding the non-dimensional expressions for thrust, torque and velocity of propeller; some basic calculations had been made in order to find out how the experimental propeller fit with the data and comparative analyses with the single screw propeller [21].

To do so, firstly it had to be calibrated the load cell. After calibration, the thrusts were measured both for single screw propulsion and coupled screw propulsion also. Then, ***"Iterative Average Theory"*** was deployed to process lots of data and to find a convergent value from them. Hence, reasonable data came to our hand to initiate the performance and efficiency calculation. In this regards, since the mechanical set up is solely dependent on electricity (DC battery), so that it was considered this as the input power. The measurement of thrusts from load cell was considered as the output power developed by the propulsion system.

When all the data were being sorted out by the Arduino console, it was also measured the instantaneous voltage (Volt.) and current draw (Ampere) by the BLDC motor deliberately. For this purpose we used a multimeter.

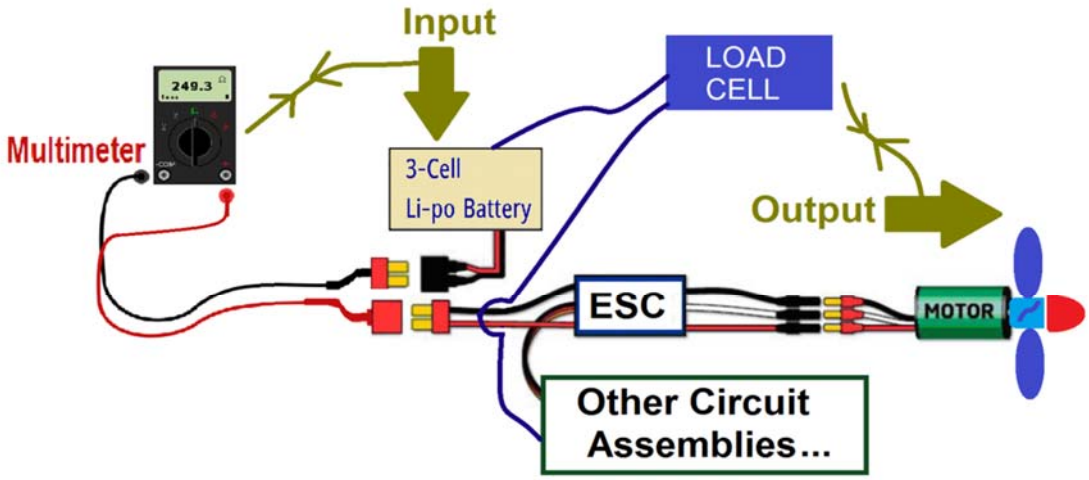

Figure 50: Measurement of consumed power and given thrust with multimeter & load-cell.

Eventually, certain numbers of experiment cycles were performed for data extraction. A schematic layout of these above methodology is illustrated above. In this experiment, it was only considered that the continuous power ratings and not any initial peak-power consumption or power drops due to continuous charge diffusion from battery were considered.

6.3 Iterative Average Theory

The theory behind the iterative mean is a process of obtaining numerical convergence in a closed data region. In the following discussion, focus will be concentrated on minimizing the number of operations required to evaluate single value by iterative technique, assuming that all arithmetic operations are exact.

Based on work of Heiko Hoffmann [17], the mean value of a distribution (X_i) can also be computed iteratively if the values $\mathbf{X_i}$ are drawn one-by-one. Let $\mathbf{(X)_t}$ be the average over the first $\mathbf{t}$ data points. It is observed that:

$$\mathbf{(X)_t} = \frac{\mathbf{1}}{\mathbf{t}} \sum_{\mathbf{i=1}}^{\mathbf{t}} \mathbf{X_i}$$

$$= \frac{\mathbf{1}}{\mathbf{t}} \sum_{\mathbf{i=1}}^{\mathbf{t-1}} \mathbf{X_i} + \frac{\mathbf{1}}{\mathbf{t}} \mathbf{X_t}$$

$$= \frac{\mathbf{t-1}}{\mathbf{t}} \cdot \frac{\mathbf{t}}{\mathbf{t-1}} \sum_{\mathbf{i=1}}^{\mathbf{t-1}} \mathbf{X_i} + \frac{\mathbf{1}}{\mathbf{t}} \mathbf{X_t}$$

$$= \frac{\mathbf{t-1}}{\mathbf{t}} \cdot \frac{\mathbf{t}}{\mathbf{t-1}} \cdot \mathbf{(X)_{t-1}} + \frac{\mathbf{1}}{\mathbf{t}} \mathbf{X_t}$$

So, the update rule for the temporary mean, $\mathbf{C\ (t+1)\ =\ (X)_t}$ upon presentation of a value $\mathbf{X}$ is given as follows:

$$\mathbf{C\ (t+1) = C\ (t) + \frac{1}{t+1} [X - C(t)]}$$

This rule is the same as for the center update in vector quantization with a learning rate that decays as $\frac{\mathbf{1}}{\mathbf{t}}$ basis. This expression was applied on data extracted for thrust developed the from load cell henceforth.

6.4 Calibration of Load Cell

As soon as the mechanical set up became operational, the load cell had been started without any load (zero thrust or pressure on the censors). The load arrays were serially shown on the screen of the Arduino console on the computer monitor. All of these readings were for zero thrust position of the load cell. After that, a known load was fixed at the pressure area of the cell (censor) and similarly lots of arrays of readings came out and all were stored as text (.txt) files for later usage. However, the known load was a Chinese solid brass made padlock of which mass was 244.0 g.

For obtaining the calibration value for no load (zero gram weight), reading were taken including **926** individual data. Some of these readings are given randomly as follows:

Table 5: Calibration of Load cell Reading (0 g)

Ser.No	Actual Reading	Iterative Average
01	297184	297184.000
02	297138	297161.000
03	296979	297039.667
04	296805	296863.667
05	296847	296850.333
06	296804	296811.722
07	296737	296747.675
08	296824	296814.459
09	296833	296830.940
10	296952	296939.894
11	297236	297209.081
12	297321	297311.673
13	297269	297272.283
14	297326	297322.163
15	297360	297357.478
16	297328	297329.842
17	297406	297401.520
150	298232	298232.738
151	298205	298205.184
152	298166	298166.258
153	298293	298292.172
154	298207	298207.553
155	297925	297926.823
156	297861	297861.422
157	297773	297773.563
158	297687	297687.548
159	297719	297718.802
160	297615	297615.649
161	297649	297648.793
162	297641	297641.048
163	297744	297743.368
164	297660	297660.508
165	297717	297716.658
166	297824	297823.353
167	297710	297710.679
168	297619	297619.546

Ser.No	Actual Reading	Iterative Average
169	297577	297577.252
170	297566	297566.066
910	297350	297350.081
911	297290	297290.066
912	297481	297480.791
913	297851	297850.595
914	297842	297842.009
915	297707	297707.148
916	297637	297637.077
917	297815	297814.806
918	298098	298097.692
919	298218	298217.869
920	298076	298076.154
921	298088	298087.987
922	298117	298116.969
923	298171	298170.941
924	298117	298117.058
925	298266	298265.839
926	298360	**298359.898**

Above all these data, the last value (**926th**) is the most convergent reading for zero gram loads.

To obtain the calibration value for known padlock load *[**Make:** SILVERLINE, **Model:** 50, **Material:** Solid Brass, **Dimension:** 50 x 41 x 16 (mm), **Weight:** 244.0 (g)]*, readings were taken including **693** individual data. Some of these readings are given randomly as follows:

Table 6: Calibration of load cell Reading (244 g)

Ser.No.	Actual Reading	Iterative Average
01	314471	314471.000
02	314473	314472.000
03	314369	314403.333
04	314146	314210.333
05	314232	314227.667
06	314473	314432.111
07	314796	314744.016
08	315002	314969.752
09	315212	315185.084
10	315242	315236.308
11	315411	315395.119

Ser.No	Actual Reading	Iterative Average
12	315744	315714.927
13	315774	315769.456
14	315748	315749.533
15	315863	315855.436
16	316124	316107.215
17	316325	316312.189
18	316259	316261.955
19	316156	316161.577
20	316157	316157.229
391	335877	335876.182
392	336322	336320.863
393	336860	336858.628
394	337449	337447.502
395	337981	337979.649
396	338519	338517.638
397	338799	338798.291
398	338524	338524.689
399	338744	338743.450
400	339163	339161.951
401	339627	339625.840
402	339664	339663.905
403	338996	338997.657
404	338253	338254.843
405	335643	335649.449
406	336517	336514.863
407	339157	339150.508
409	338089	338090.967
410	335317	335323.766
680	334404	334402.542
681	335275	335273.719
682	336175	336173.678
683	337344	337342.286
684	337780	337779.360
685	337648	337648.192
686	336776	336777.271
687	335652	335653.638
688	335040	335040.892
689	334969	334969.104
690	334607	334607.525
691	334118	334118.708
692	333768	333768.507
693	333566	**333566.292**

Above all these data, the last value (**693th**) is the most convergent reading for lock's known mass as 244.0 g weight.

Having these two values were written down as final for the purpose of numerical calculation of other loads (i.e. unitary method, interpolation or extrapolation, etc.). If it is to say, any load shown by load cell is $\mathbf{X_{L.C.}}$, then the equivalent load value will be calibrated such like this:

Table 7: Interpolation for X value

Ser.No.	Reading (Unitless)	Load (g)
1	298359.8983	0
2	333566.2922	244.0
3	$X_{L.C.}$	$X_{L.C.} \times \left\{\frac{333566.2922-298359.8983}{244-0}\right\}$

Henceforth the value of multiplier for, $\mathbf{X_{L.C.}}$ is = *144.288* (approx.)

6.5 Performance Investigation of Single Screw

When the single screw was started to propel in calm water of tank filled with fresh water, it gave thrust readings with respect to the related revolution speed in percentage (%) according to the BLDC motor's maximum possible revolution per minute (rpm).

6.5.1 Data Mining & Curve Generation

Total **2293** nos. readings were taken which were distributed in variable speed ranges. Among all these, randomly picked data from each steady speed range (i.e. 10%, 20%, etc.) are given:

Table 8: Thrust Reading for Single Screw

Ser.No.	Raw Data	Speed (%)	Calibrated Data	Iterative Average
01	70223	0	486.781	486.781
02	70180	0	486.483	486.632
03	70183	0	486.504	486.497
33	70165	0	486.379	486.378
34	70201	0	486.628	486.621

Ser.No.	Raw Data	Speed (%)	Calibrated Data	Iterative Average
35	70185	0	486.517	486.521
36	***70224***	***0***	***486.788***	***486.780***
76	70164	10	486.372	486.373
77	70157	10	486.323	486.324
78	70157	10	486.323	486.323
79	70139	10	486.199	486.200
80	70131	10	486.143	486.144
81	***70118***	***10***	***486.053***	***486.054***
149	70088	20	485.845	485.847
150	70092	20	485.873	485.873
151	70154	20	486.303	486.300
152	***70201***	***20***	***486.628***	***486.626***
153	70196	30	486.594	486.594
154	70160	30	486.344	486.346
155	70089	30	485.852	485.855
218	70066	30	485.692	485.694
219	70080	30	485.790	485.789
220	70117	30	486.046	486.045
221	70085	30	485.824	485.825
222	***70073***	***30***	***485.741***	***485.741***
327	70079	40	485.783	485.782
328	70079	40	485.783	485.783
329	70053	40	485.602	485.603
330	70089	40	485.852	485.851
332	***70079***	***40***	***485.783***	***485.783***
411	59572	50	412.949	413.020
412	55871	50	387.294	387.356
413	56489	50	391.578	391.567
414	52630	50	364.827	364.892
415	52590	50	364.550	364.551
416	53319	50	369.603	369.591
417	***53279***	***50***	***369.326***	***369.327***
2186	57733	50	400.201	400.212
2187	55811	50	386.878	386.884
2188	55747	50	386.434	386.434
2189	55770	50	386.594	386.594
2190	56040	50	388.465	388.464
2191	***56065***	***50***	***388.639***	***388.638***
2231	65500	40	454.041	454.038
2232	66182	40	458.769	458.767
2233	64909	40	449.945	449.948
2234	63748	40	441.897	441.900

Ser.No.	Raw Data	Speed (%)	Calibrated Data	Iterative Average
2235	64372	40	446.222	446.220
2236	***65905***	***40***	***456.849***	***456.844***
2288	71410	30	495.009	495.008
2289	71164	30	493.304	493.305
2290	70836	30	491.030	491.031
2291	71032	30	492.389	492.388
2292	71412	30	495.023	495.022
2293	***71313***	***30***	***494.337***	***494.337***

From the readings above, the selected values of thrust from a particular speed ranges for single screw propeller had been illustrated below and hence performance curve is generated thereby:

Table 9: Thrust vs. Speed % for Single Screw

	Speed (rpm %)	Thrust (g)	Iterative Thrust (N)
Rise	0	486.787	4.780
	10	486.053	4.773
	20	486.628	4.779
	30	485.741	4.770
	40	485.783	4.770
	50	369.326	3.627
Fall	50	388.639	3.816
	40	456.848	4.486
	30	494.336	4.854

The performance curve for single screw propeller is given below and this is generated with respect to the data provided in the table above, thrusts vs. speed respectively:

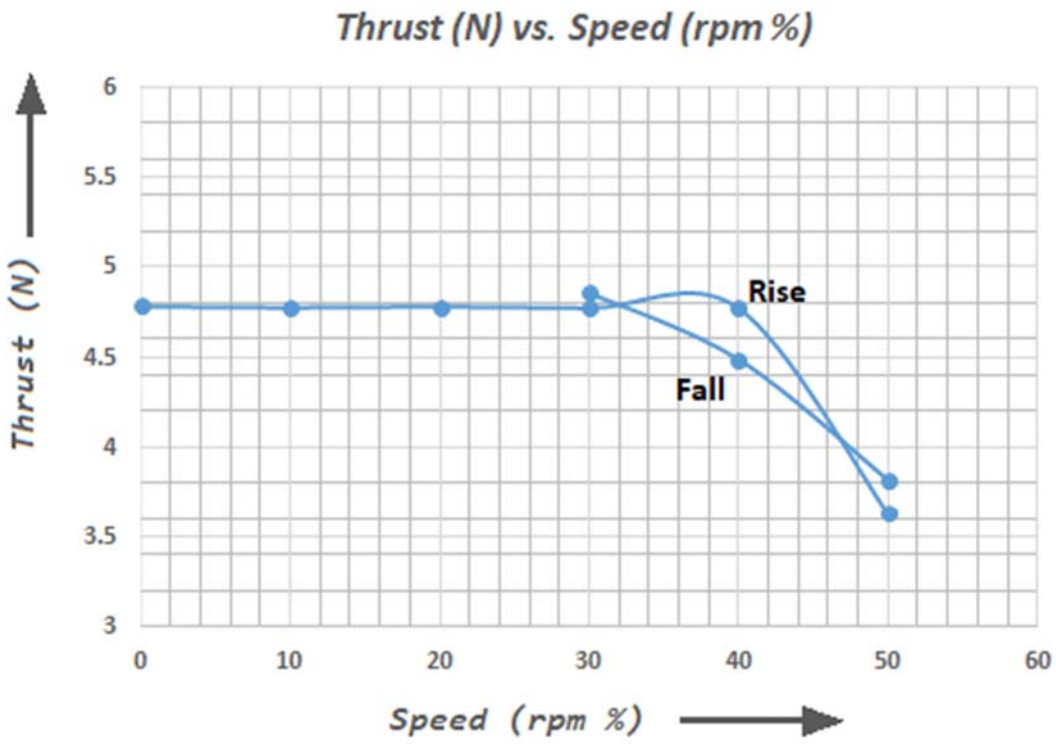

Figure : 51 Thrust (N) vs. Speed (rpm %) Curve for Single Screw

6.5.2 Performance Calculation

This calculation process stands on some basic formula and methodologies. In briefly, BLDC generated propeller thrust is always proportional to the current diffused by the LiPo battery pack. So, it had been found out all the data below for powering calculation and efficiency determination [22].

1. Description that inscribed in the manual of BLDC motor states that it is of **930 kV**, which means 930 rpm is equivalent to unit voltage input or fluctuates per unit voltage ups and downs. So, for input of **10 Volts** at the point from where the BLDC motor wires draw currents (**5 Amps.**) from LiPo Battery,

It was observed, the number of rpm = (930 **X** 10) rpm = **9300 rpm**.

[This rpm is applicable when the model operates at 100% of its speed of advance] [23]

2. On the other hand, some formula from rotational dynamics had been used to determine some of the outputs of the motor as well as the propellers. Calculated values from using these rotational dynamic formulas had also been used afterwards to generate the values for advance coefficient, power and torques.

3. Following data were used to construct the below table of performance [24],

r = propeller radius

= (11.31 ÷ 1000) m

= 0.01131 m

$\mathbf{V_s}$ = Model's estimated speed

= (w x r) ms^{-1}

= $\mathbf{\left(2\pi \times \frac{rpm}{60} \times r \right)}$ ms^{-1}

ρ = Density of fresh water

= 1000 kgm^{-3}

P = Horse Power

= **{(Volt x Ampere) ÷ 746} HP**

= {(10V x 5 Amps.) ÷ 746}

= 0.067 HP

$\mathbf{Q_{SS}}$ = Torque

= **(5252 x P) ÷ rpm**

= 351.884 ÷ rpm

4. On the basis of above data, below table of data emerges forward for investigating the performance of single screw propeller:

Table 10: Performance Table for Single screw

	% of Speed	RPM (min^{-1})	Speed (ms^{-1})	Thrust (N)	Torque (Nm)	Advance Coeff.	Thrust Coeff.	Torque Coeff.	Efficiency
	(%S)	(n)	(V_S)	(T)	(Q_{ss})	(J_a)	(K_T)	(K_Q)*	(η)
Rise	0	0	0	4.780	-	-	-	-	0.0143
	10	930	1.102	4.773	0.378	3.142	0.02108	0.7387	0.0571
	20	1860	4.406	4.779	0.189	6.283	0.00528	0.0923	0.1283
	30	2790	9.913	4.770	0.126	9.425	0.00234	0.0274	0.2281
	40	3720	17.624	4.770	0.095	12.566	0.00132	0.0115	0.2710
	50	***4650***	***27.537***	***3.627***	***0.076***	***15.708***	***0.00064***	***0.0059***	***0.2852***
Fall	50	4650	27.537	3.816	0.076	15.708	0.00067	0.0059	0.2146
	40	3720	17.624	4.486	0.095	12.566	0.00124	0.0115	0.1306
	30	2790	9.913	4.854	0.126	9.425	0.00238	0.0274	0.0143

* *For plotting of graph purpose, torque coefficient is taken as* $K_Q = 10K_q$

5. From above table, the efficiency had to be calculated. Taking a random operation at 50% speed (at rising rpm = 4650) of the BLDC motor into consideration, it was sorted out that the propeller efficiency as,

$$\eta = \frac{J_a}{2\pi} \cdot \frac{K_T}{K_Q}$$

$$= \frac{15.708 \text{ X } 0.00064}{2 \text{ X } 3.1416 \text{ X } 0.00059}$$

$$= 0.2852$$

$$= \mathbf{28.52\%}$$

6.6 Performance Investigation of Coupled Screw

Similarly as previous, the coupled screw started to propel in calm water of tank filled with fresh water, it gave thrust readings with respect to the related revolution speed in percentage (%) according to the BLDC motor's maximum possible revolution per minute (rpm).

6.6.1 Data Mining & Curve Generation

Total **1230** nos. readings were taken which were distributed in variable speed ranges. Among all these, randomly picked data from each steady speed range (i.e. 10%, 20%, etc.) are given below:

Table 11: Thrust Reading for coupled screw

Ser. No.	Raw Data	Speed (%)	Calibrated Data	Iterative Average
1	69652	0	482.823	482.823
2	69629	0	482.663	482.743
35	69705	0	483.190	483.200
36	69707	0	483.204	483.204
37	69603	0	482.483	482.503
38	68677	0	476.064	476.233
39	***68673***	***0***	***476.036***	***476.037***
65	69728	10	483.350	483.358
66	69040	10	478.580	478.653
67	68467	10	474.608	474.668
70	69785	10	483.745	483.741
72	***69824***	***10***	***484.015***	***484.016***
136	69855	20	484.230	484.230
142	69919	20	484.674	484.672
143	69883	20	484.424	484.426
144	69457	20	481.471	481.491
145	68515	20	474.941	474.986
146	69174	20	479.509	479.478
147	69832	20	484.070	484.039
148	***69865***	***20***	***484.299***	***484.298***
194	69867	30	484.313	484.312
195	69907	30	484.590	484.589
202	68559	30	475.246	475.265
203	69495	30	481.734	481.702
204	69843	30	484.147	484.135
205	***69884***	***30***	***484.431***	***484.430***

Ser. No.	Raw Data	Speed (%)	Calibrated Data	Iterative Average
290	69976	40	485.069	485.068
291	69969	40	485.020	485.020
295	70048	40	485.568	485.567
298	70005	40	485.270	485.271
299	69965	40	484.992	484.993
300	***69975***	***40***	***485.062***	***485.061***
301	***70008***	***50***	***502.087***	***502.071***
302	69991	50	485.173	485.173
303	69339	50	480.653	480.668
304	68314	50	473.548	473.571
1100	71622	50	496.479	496.474
1104	71226	50	493.734	493.736
1105	70095	50	485.894	485.901
1106	70120	50	486.067	486.067
1107	69649	50	482.802	482.805
1108	69975	50	485.062	485.060
1109	***72431***	***50***	***485.290***	***485.290***
1159	71599	40	496.319	496.319
1160	71584	40	496.215	496.215
1161	71545	40	495.945	495.945
1166	71575	40	496.153	496.154
1167	71465	40	495.390	495.391
1168	***71509***	***40***	***495.695***	***495.695***
1221	70900	30	491.474	491.471
1222	71700	30	497.019	497.015
1223	71678	30	496.867	496.867
1226	71515	30	495.737	495.737
1227	71604	30	496.354	496.353
1228	71660	30	496.742	496.742
1229	71696	30	496.992	496.991
1230	***71657***	***30***	***496.721***	***496.721***

From the readings above, the selected values of thrust from a particular speed ranges for coupled screw propeller had been illustrated below and hence performance curve is generated thereby:

Table 12: Thrust vs. Speed % table for coupled screw

	Speed (%)	Thrust (g)	Iterative Thrust (N)
Rise	0	476.036	4.675
	10	484.014	4.753
	20	484.299	4.756
	30	484.431	4.757
	40	485.062	4.763
	50	502.087	4.930
Fall	50	485.29	4.766
	40	495.695	4.868
	30	496.721	4.878

The performance curve for coupled screw propeller is given below and this is generated with respect to the data provided in the table above, thrusts vs. speed respectively:

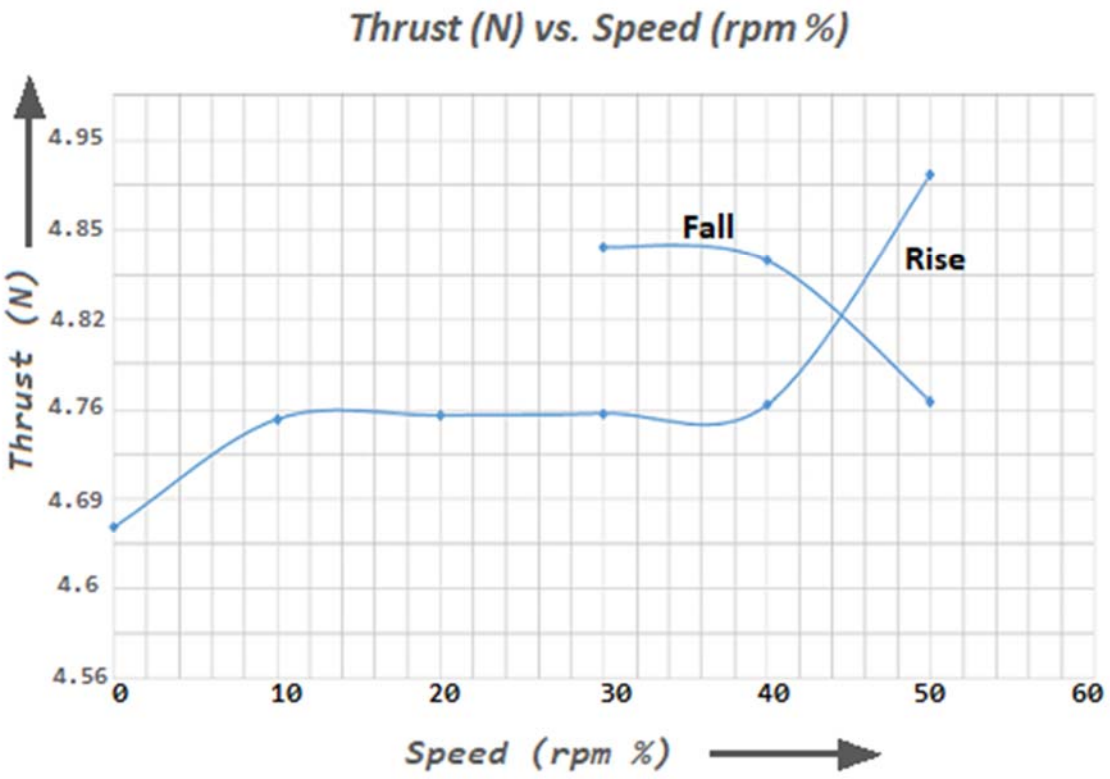

Figure : 52 Thrust (N) Vs. Speed (rpm%) Curve for Coupled Screw

6.6.2 Performance Calculation

This calculation process stands on some basic formula and methodologies. In briefly, BLDC generated propeller thrust is always proportional to the current diffused by the LiPo battery pack. So, it had been found out all the data below for powering calculation and efficiency determination for coupled screw system.

1. Description that inscribed in the manual of BLDC motor states that it is of **930 kV**, which means 930 rpm is equivalent to unit voltage input or fluctuates per unit voltage ups and downs. So, for input of **8.82 Volts** at the point from where the coupled BLDC motor wires draw currents (**4.65 Amps.**) from LiPo Battery, [24]

   The number of rpm = (930 **X** 8.82) rpm = **8202.6 rpm**.

   [This rpm is applicable when the model operates at 100% of its speed of advance]

2. On the other hand, some formula from rotational dynamics had been used to determine some of the outputs of the motor as well as the propellers. Calculated values from using these rotational dynamic formulas had also been used afterwards to generate the values for advance coefficient, power and torques [25].

3. Following data were used to construct the below table of performance,

   r = propeller radius

   = (11.31 ÷ 1000) m

   = 0.01131 m

   $\mathbf{V_s}$ = Model's estimated speed

   = (w x r) ms^{-1}

   = $\mathbf{\left(2\pi \times \frac{rpm}{60} \times r \right)}$ ms^{-1}

   ρ = Density of fresh water

   = 1000 kgm^{-3}

   P = Horse Power

   = **{(Volt X Ampere) ÷ 746} HP**

= {(8.82V x 4.65 Amps.) ÷ 746}

= 0.055 HP

$\mathbf{Q_{CS}}$ = Torque = **(5252 x P) ÷ rpm =** 288.86 ÷ rpm

4. On the basis of above data, below table of data emerges forward for investigating the performance of single screw propeller:

Table 13: Performance Table for Coupled Screw

	% of Speed	RPM (min^{-1})	Speed (ms^{-1})	Thrust (N)	Advance Coeff.	Torque (Nm)	Thrust Coeff.	Torque Coeff.	Efficiency
	(%S)	(n)	(V_s)	(T)	(J_a)	(Q_{CS})	(K_T)	(K_Q)*	(η)
Rise	0	0	0.000	4.675	-	-	-	-	-
	10	820.26	0.972	4.753	3.142	0.352	0.0270	0.8838	0.0153
	20	1640.52	3.886	4.756	6.283	0.176	0.0067	0.1105	0.0611
	30	2460.78	8.744	4.757	9.425	0.117	0.0030	0.0327	0.1375
	40	3281.04	15.544	4.763	12.566	0.088	0.0017	0.0138	0.2448
	50	***4101.3***	***24.288***	***4.930***	***15.708***	***0.070***	***0.0011***	***0.0071***	***0.3959***
Fall	50	4101.30	24.288	4.766	15.708	0.070	0.0011	0.0071	0.3826
	40	3281.04	15.544	4.868	12.566	0.088	0.0017	0.0138	0.2501
	30	2460.78	8.744	4.878	9.425	0.117	0.0031	0.0327	0.1410

* *For plotting of graph purpose, torque coefficient is taken as* $K_Q = 10K_q$

5. From above table, the efficiency had to be calculated [26]. Taking a random operation at 50% speed (at rising rpm = 4101.3) of the coupled BLDC motor into consideration, it was sorted out that the propeller efficiency as,

$$\eta = \frac{J_a}{2\pi} \cdot \frac{K_T}{K_Q}$$

$$= \frac{15.708 \text{ X } 0.00112}{2 \text{ X } 3.1416 \text{ X } 0.00707}$$

$$= 0.3959$$

$$= \mathbf{39.59\ \%}$$

6.7 Comparative Performance Analyses

Analytical comparison between single screw and coupled screw propeller might have numerous factors to influence the efficiency. Water pressures, wave characteristics, power generation method, density of water, resistance of the propeller mountings, tension and compression of the urethane belt drive, etc. are the most prominent ones among all of these factors.

Taking all these conditions into consideration, it was observed that coupled screw model performance is slightly greater than the existing single screw propulsion device. This experiment showed that, the effectiveness of the mechanical set up has been increased to **(39.59 – 28.52) %** or, **11.07%**, which is higher to a certain extent than the single screw.

Observing the results through another approach, what has been calculated is much more similar to what have just been found out above. In details, if the $\mathbf{K_T}$, $\mathbf{K_Q}$ and efficiency ($\boldsymbol{\eta}$) data generated by both of these propellers are plotted against the advance coefficients ($\mathbf{J_a}$) of the B.L.D.C motor, then the below curves will be generated eventually:

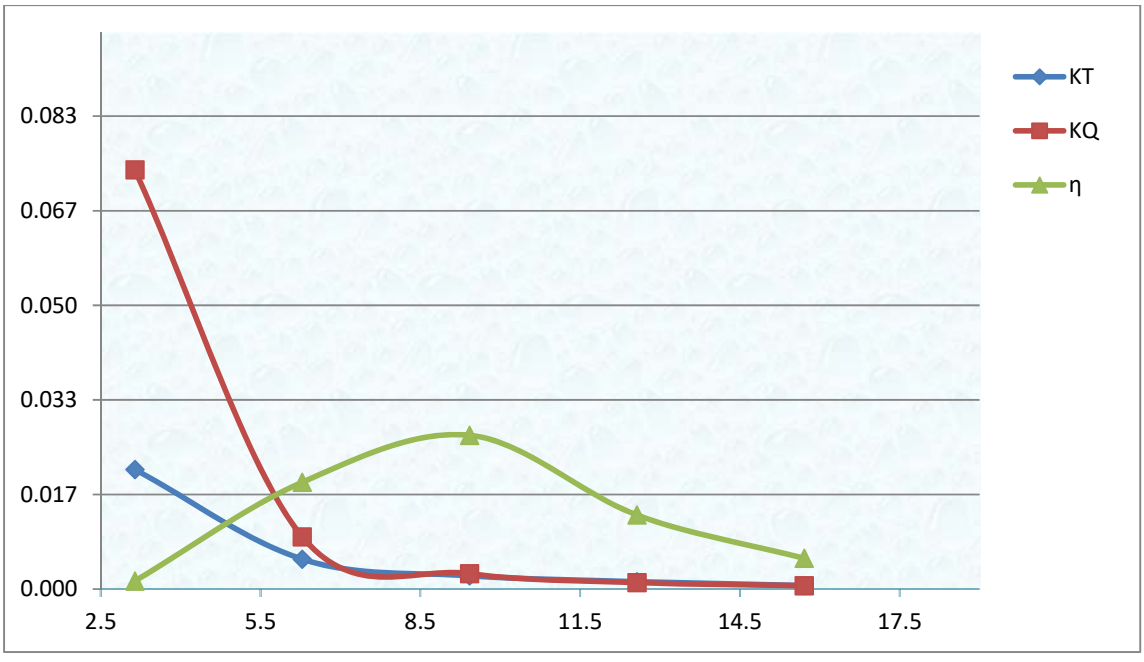

Figure 53: Propeller Efficiency Curves for Single Screw

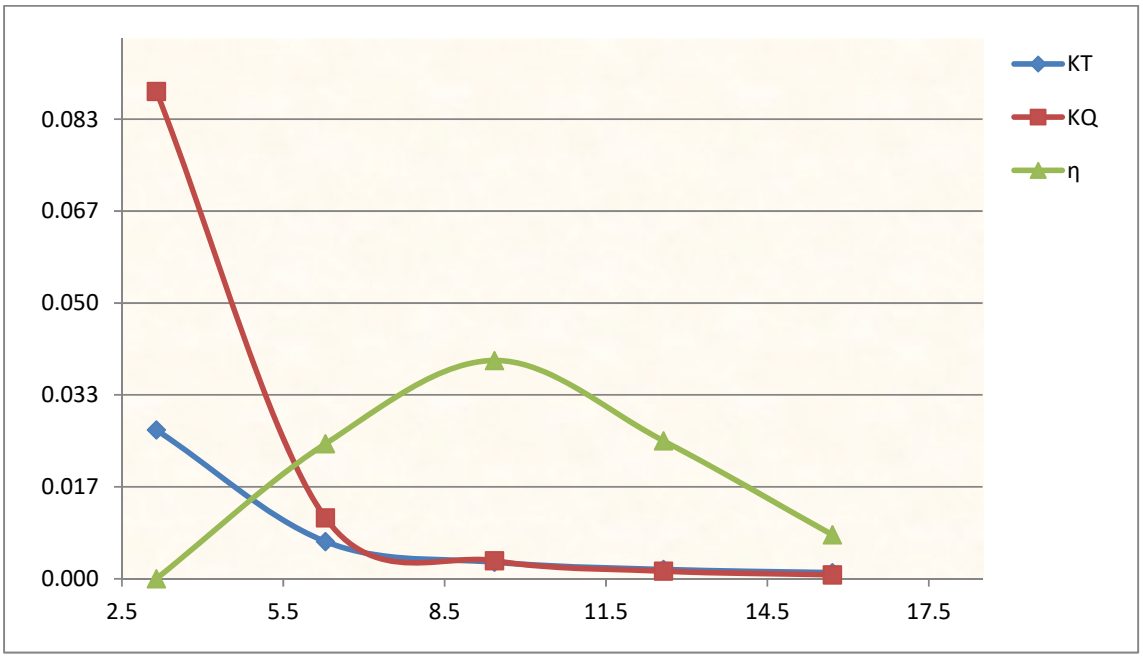

Figure 54: Propeller Efficiency Curves for Coupled Screw

Plotted graph and the comparison of data, are complying that for the randomly picked operation at 50% speed, the increment of the efficiency is **11.07%** approximately. The deviation of any sort of percent neither invalidates all the data analyses in this thesis nor suggests the derived formula for coupled screw to be mathematically errorless.

Chapter : 07

CONCLUSION AND RECOMMENDATION

7.1 Conclusion

This thesis covers the process of mechanical investigation of the water tank test for a ship propeller. Two different approaches were applied for both of the propulsion system; one is mathematical and the other is electro-mechanical, the results of which are compared with experimental data in order to evaluate their effectiveness. The single screw propeller is estimated to be less effective than the coupled screw propeller in regards to power thrust delivery from the consumed power by nearly **11%** more or less.

If this test would run in a fully privileged towing tank facility, then the experimental results would have been more accurate so that it could be specified the effectiveness of the coupled screw propeller in a more accurate way. Most of the time during the experiment, data and readings were taken manually by hand; which caused problems in obtaining data structures and hence generating tables in order to plot different type of efficiency graphs. All constraints would be minimized if the whole process of propulsion was initiated in a towing tank. Nevertheless, the experiment showed a result which could not be neglected as the result is based on rigid statistical platform.

7.2 Recommendation

In near future, some sort of experiments can be operated for examining some objectives regarding the coupled screw propulsion. In example, this whole process which had already been done in this thesis can also be experimented through CFD simulation in open water characteristics. Additionally, coupled screw propulsion should also be checked of its effectiveness or efficiency with the twin screw propulsion system and this is the next doable project that should check the percentage of difference in efficiency with the twin screw.

Moreover, in this experiment, the loss of energy due to the slip of urethane belt was not considered. This should also be incorporated in further scopes of the thesis with the inclusion of the equations of belt, chain and rope.

A major field of maneuvering is not experimented due to its physical absence in propulsion theories as well as in industries. This major field is “Rudder”. As the propulsion device is uncommon, so that there might be a better scope of giving theory or inventing geometry for a new type of rudder to maneuver coupled screw system. Also, ducted concept can be applied on this propulsion device by using elliptical Kort Nozzle all around the coupled screw belt. This thesis also has some future scopes related to propeller geometry, wake profile, resistance due to lateral motion over the belt, effect of skew, rake and controllable pitch, etc. As time was scarce for the partial fulfillment of the baccalaureate degree, the thesis was solely focused on comparative analyses of efficiency criteria.

At the end, it is a matter of wishing that, if all of these future scopes become experimented gradually then a competitive sets of unique theories, equations and a large database can be established for research and development purpose in the field of invention of innovative, cost efficient and applicable propulsion systems.

REFERENCES

[1] N.W. Prench, *United States Patent No: US413852*, Dated: Jan 29, 1889.

[2] E.N. Kerr, *United States Patent No: US988112*, Dated: Mar 28, 1911.

[3] Holsez, *United States Patent No: US8939104 B2*, Dated: Jan 27, 2015.

[4] *The Shorter Science and Civilization in China* by Joseph Needham, Colin A. Ronan, Cambridge University Press, 1978 ISBN 0-521-31560-3, ISBN 978-0-521-31560-9.

[5] Ghose, J.P., Gokarn, R.P., *Basic Ship Propulsion.*

[6] Harvald, S.A., *Resistance & Propulsion of Ships.*

[7] Paul Augustin Normand, *La Genèse de l'Hélice Propulsive (The Genesis of the Screw Propulsor)*. Paris: Académie de Marine, 1962, pp. 31–50.

[8] Carlton, J., *Marine Propellers and Propulsion,* (3rd Edition), Elsevier 2012 Ed.

[9] Smith, Edgar C. , *A Short history of Naval and Marine Engineering* , 1905, University Press, Cambridge. pp. 66–67.

[10] *Propeller Characteristics With Different Locations Of The Rudders In The Propeller Race Of Twin Rudders -Twin Screw Ships* (K. Kafali, May 1961, DOI: 10.1111/ j.1559-3584.1961.tb03310.x) ,

[11] Strom Tejsen, J., Robert Roddy Jr., F., *Performance of container ship with overlapping propeller arrangement.*

[12] Hadler, J.B. et al*, Contra-rotating Propeller Propulsion-A State of the Art Report.*

[13] *Study of Propeller Blade Stresses and Bearing Forces on A High Speed Twin-Screw Container Ship* (H. Okamoto, K. Nozawa, T. Umakoshi, June 1976) .

[14] Goldstein, S., *On the Vortex Theory of Screw Propellers*, Proceedings of the Royal Society of London. Series A, Containing Papers of a Mathematical and Physical Character, Volume 123, Issue 792, pp. 440-465.

[15] Kenneth, M., Clarke, J., *Experimental characterization of alternative propeller designs,* Dept. of Mechanical Engineering, University of Strathclyde (2009).

[16] A. Coraddu a, G. Dubbioso b, S. Mauro b, M. Viviania n., *Analysis of twin screw ships' asymmetric propeller behavior by means of free running model tests,* University of Genoa, DITEN, Naval Architecture Unit, Via Montallegro 1, 16145 Genova, Italy.

[17] Heiko Hoffmann, *Unsupervised Learning of Visuomotor Associations,* Ch-A.3 (Iterative Mean), MPI Series in Biological Cybernetics, Vol. 11, Logos Verlag Berlin, ISBN 3-8325-0858-9.

[18] *Grayson Hobby-A2212/13T-1000Kv,* B.L.D.C. Motor Datasheet, Suppo Ltd.

[19] www.arduino.cc

[20] *3133 - Micro Load Cell (0-5kg) - CZL635*, Datasheet - May 13, 2011.

[21] Aung Ko Latt, *Numerical Investigation of Propulsion Efficiency Depending on Propeller Position*, Master Thesis, University of Roschtock, Germany (EMSHIP: 2015-17).

[22] Muntean, T.V., *Propeller efficiency at full scale : measurement system and mathematical model design*, Technische Universiteit Eindhoven, DOI:10.6100/IR723143, Published: 01/01/2012.

[23] www.micromo.com/technical-library/dc-motor-tutorials/motor-calculations

[24] National Energy Management Institute Committee © 2005, United States

[25] Mogens Blanke et al, *Dynamic Model For Thrust Generation Of Marine Propellers*, Department of Automation, Technical University of Denmark, DK-2BOO Kgs. Lyngby, Denmark.

[26] Douglass, John G., *Efficacy of Methods for Estimating In-Service Motor Efficiency,* Washington State University Cooperative Extension Energy Program report prepared for the Pacific Gas and Electric Company and the Bonneville Power Administration, June 1997.